

Spring 5-19-2017

Growth laws for sub-delta crevasses in the Mississippi River Delta: observations and modeling

Tara A. Yocum
University of New Orleans, tyocum@uno.edu

Follow this and additional works at: <https://scholarworks.uno.edu/td>



Part of the [Hydrology Commons](#), and the [Sedimentology Commons](#)

Recommended Citation

Yocum, Tara A., "Growth laws for sub-delta crevasses in the Mississippi River Delta: observations and modeling" (2017). *University of New Orleans Theses and Dissertations*. 2339.
<https://scholarworks.uno.edu/td/2339>

This Thesis is protected by copyright and/or related rights. It has been brought to you by ScholarWorks@UNO with permission from the rights-holder(s). You are free to use this Thesis in any way that is permitted by the copyright and related rights legislation that applies to your use. For other uses you need to obtain permission from the rights-holder(s) directly, unless additional rights are indicated by a Creative Commons license in the record and/or on the work itself.

This Thesis has been accepted for inclusion in University of New Orleans Theses and Dissertations by an authorized administrator of ScholarWorks@UNO. For more information, please contact scholarworks@uno.edu.

Growth laws for sub-delta crevasses in the Mississippi River Delta: observations and modeling

A Thesis

Submitted to the Graduate Faculty of the
University of New Orleans
in partial fulfillment of the
requirements of the degree of

Master of Science
in
Earth and Environmental Science

by

Tara Ann Elizabeth Yocum

B.S University of New Orleans, 2014

May, 2017

Copyright 2016, Tara Yocum

Acknowledgments

This thesis would not have been possible without the combined efforts of many. First and foremost, I would like to thank my major professor, Dr. Ioannis Georgiou for mentoring me throughout this process. You have opened opportunities for me I never conceived were possible. Your passion and love for science is contagious and appreciated. I owe you a debt of gratitude for the hours you spent helping me understand concepts and the abundance of questions you so patiently answered. My committee members Dr. Kyle Straub and Dr. John McCorquodale, for your time, expertise and advice during this research. An extra thanks to Dr. Kyle Straub for providing the experimental deltas used in this work and helping me with MatLab. The efforts of an amazing field team made the field deployment and sample collection possible, even though weather didn't always permit; Mike Brown, Geoff Udoff, Trey Kramer, and Christopher Esposito. I would like to thank Zoe Hughes, for lending us instrumentation. To Brittany Kime, Kevin Hanegan, Ahmed Gaweesh, and Josh Flathers your patience and advice while I was learning Delft3D was invaluable and Kevin Trosclair for your help initiating this work during my undergraduate years. I also need to thank Sunni Siqueira and Rachelle Thomason you provided a tremendous amount of guidance and encouragement over the past two years. Finally, my gratitude goes to my mom, Lisa Jamieson and friend, Penny Lemoine for the numerous times you read my thesis and your unwavering belief in me even when stress got the best of me. I cannot begin to describe how grateful I am for every single person that has helped me through this amazing journey. Thank you!

Contents

List of Figures.....	VI
Abstract.....	X
1 Introduction.....	1
2 Hypotheses	8
3 Material and Methods	9
3.1 Planform Metrics and Growth Laws	9
3.2 Field Data Collection	12
3.3 Hydrodynamic Analysis	15
3.4 Sedimentological Analysis	16
3.5 Numerical Modeling	16
3.5.1 Model Grid and Basin Design	18
3.5.2 Initial and Boundary Conditions	19
3.5.3 Model experimental design	20
4 Results	22
4.1 Planform	22
4.2 Delta Allometry.....	23
4.3 Width Depth Ratio	25
4.4 Hydrodynamic.....	26
4.5 Sedimentological.....	29

4.6 Depositional Mechanics	31
4.7 Sediment Retention	34
5 Discussion.....	37
6 Conclusions.....	42
References	43
Appendix A	50
Vita	54

List of Figures

- Figure 1: Map of the study area within the Mississippi River Delta, MR-09 projects (06, 09, 11, 12, 15, 20, 31, 36, 38, 51, and OP-5 UDC), USFWS projects (92-5 DC, 93-1, and 83-1), and Brant's Splay. Image from Google Earth. 7
- Figure 2: Bifurcation widths and lengths to bifurcation order (left). The developed crevasse (92-5) delta allometry metrics from Wolinsky et. al. (2010; right). Images from Google Earth. 10
- Figure 3: Experimental deltas from Tulane Universities Department of Earth and Environmental Sciences Sediment Dynamics Laboratory. (Left) Experiment TDB-12 (Right) and TDB-13 (Straub et al., 2015)..... 11
- Figure 4: (A) Deployment locations of Aqua A, Aqua B, and the RBR as well as ADCP transect locations (blue and green lines). The green and blue lines indicate transects that were made at 11AM and the blue lines only indicate transects that were made at 4PM. (B) Core locations are indicated with green stars. Surface water and grab samples are indicated with red arrows and green stars. Images A and B from Google Earth. (C) Me on the kayak about to collect cores in the UDC. 14
- Figure 5: Model grid (black lines), basin design and boundaries (red lines) for the SS, FB and HB. 19

Figure 6: (A) Non-dimensional distance to the river mouth bar (L/D) to JMF. Light green, open red circles and black power trend were digitized from Edmonds and Slingerland (2007) with measured data from SDC (open purple), Brant’s Splay (solid dark green), AD (solid red), WLD (solid orange), TDB_12 (dark blue), and TDB_13 (light blue). Dotted gray lines represent 80% confidence. Non-dimensional channel geometries width (B), depth (C), and length (D) for Edmonds and Slingerland (2007) deltas (green), SDC (purple), TDB_12 (dark blue), and TDB_13 (light blue) as a function of bifurcation order with exponential trends. 23

Figure 7: Delta allometry digitized from Wolinsky et al. (2010) (blue, gray, and green dashed lines and red circles). (A-C) Delta allometry for six SDC (purple), and (D-F) TDB_12 (dark blue), and TDB_13 (light blue). 24

Figure 8: Width depth relationship digitized from Howes et al. (2012) (dark red and light green circles) with SDC (purple), Brant’s Splay (dark green), AD (light red), WLD (orange), TDB_12 (dark blue), and TDB_13 (light blue). 25

Figure 9: (A) Location of tide gauges and deployment locations. (B) Tide (m) within UDC and DC; AquaPro A (blue line) AquaPro B (red line) and RBR (green line). Tide gauge data from Pilottown (purple), CRMS4448 (dotted gray) and CRMS4626 (solid gray). Image from Google Earth..... 26

Figure 10: (A-C) Flow (m^3/s) distribution on April 2, 2015, and on February 19, 2016 (~11am and 4pm). Blue arrows indicate measured flows while green is calculated by the difference in flow upstream and downstream of the location. (D) Water levels from the RBR (green), CRMS 4626 (gray) and NOAA Pilottown, LA (purple) on February 18th

to February 19th. ADCP transects began at 11AM (solid black line), and ended after 4PM (dashed black line). Images from Google Earth..... 27

Figure 11: (A) Discharge from Belle Chasse, LA in thousands of m³/s (gray) with the extrapolated discharge for the UDC (orange) and DC (blue) in m³/s. The dashed and solid black lines are the start and end times of measured data from deployments. (B) The UDC (orange) and DC (blue) discharge during the time of the deployment window with the Belle Chasse discharge (gray)..... 28

Figure 12: Results from sediment analysis. (A) Total SSC (mg/L) throughout the developed and undeveloped sub-delta crevasse and along Octave Pass. Blues represent lower concentrations with higher concentrations represented in red. (B) D₅₀ (μm) throughout the DC and UDC and along Octave Pass. Sand sized material (red, greater than 61μm), silt (green, 61μm to 4μm), and clay sized material (blue, less than 4μm). (C) Photographs of cores and (D) their locations within the undeveloped crevasse. (E) Sand (dotted lines, secondary y-axis) and mud (solid lines, primary y-axis) discharge into the DC (blue) and UDC (orange) in kg/s during the deployment window (dashed and solid black lines). Images from Google Earth..... 30

Figure 13: Relative sediment deposition volume including morph factor along the centerline of the basin for each sediment supply characteristic (SSC130, 20% sand [blue], SSC130, 5% sand [red], SSC100, 20% sand [green], SSC75, 20% sand [purple]). (A) Q_c and WL_c for each accommodation depth (1m, 1.5m, and 2m) in the SS. (B) Four scenarios 1) Q_c and WL_c, 2) Q_c, WL_c, 3) Q_c and WL_c, and 4) Q_c and WL_c with constant depth (2m) in the FB. (C) Sediment deposition in the 1m SS with TSS concentration 100 mg/l according the same four scenarios in B. 32

Figure 14: Relative sediment deposition volume including morph factor along the centerline of the basin per each sediment supply characteristic (SSC130, 20% sand [blue], SSC130, 5% sand [red], SSC100, 20% sand [green], SSC75, 20% sand [purple]). (A) Q_c and WL_c for each accommodation depth (1m, 1.5m, and 2m) in the FB. (B) Q_c and WL_c for each accommodation depth (1m, 1.5m, and 2m) in the HB. 33

Figure 15: The evolution of sediment deposition in the 1m SS basin through out the simulation (1st, 2nd, 3rd and 4th quarters). 34

Figure 16: Sediment retained by percent (y-axis) and volume (secondary y-axis, yellow diamond) of total sediment input. Columns colors indicate what percent of the total percent sediment retained is sand (gray), silt (orange) or clay (green). Columns are further arranged by basin depth (1.5m and 2m), simulation type (Q_c , Q_{\sim} , WL_c , WL_{\sim}) and sediment condition at the input boundary (SSC, and % sand). 35

Figure 17: Fifteen-day simulation results using the end and half way points of the 1m SS, 1m and 1.5m FB simulations. 36

Figure 18: Length to depth relationship for AD (red), WLD (orange), Brant’s Splay (BS; green), SDC (purple), TDB_12 (dark blue), and TDB_13 (light blue). Open circles indicate when the predicted length ($L_{RMB/D}$) was shorter than the measured (L/D). The solid circles indicate when the predicted was longer than measured. The black line on the secondary x and y-axis is the Edmonds and Slingerland (2007) trend. 39

Figure 19: The SDC (12, 20, 31 and 51; A-D) and Brant’s Splay (E), showcasing the low number of bifurcations and channel lengths. 40

Abstract

In this study we assessed growth laws of sub-delta crevasses in the Mississippi River delta plain, experimental laboratory deltas, and compared them to previously studied river dominated large deltas worldwide. Metrics for channel and delta geometry for each system were obtained using a combination of geospatial tools, bathymetric datasets, sediment size, and hydrodynamic observations. Most crevasses and experimental deltas appear to obey delta growth laws suggesting that they exhibit planform metrics similar to larger deltas. However, some channels within each system, exhibit outlier behavior (e.g. asymmetric growth) where channel length is much larger than channel width. Hydrodynamic observations and morphodynamic modeling results, support the role of confinement in governing this response, through direct lateral confinement of the receiving basin width and depth thus guiding channels, and indirect confinement caused by sediment cohesion, whereby natural levees guide the systems asymmetric channel growth.

Keywords: Crevasses, River Deltas, Delta Growth Laws, Delft3D, Delta Allometry, Wetland Loss, Mississippi River Delta

Introduction

River deltas are among the most important interfaces on Earth. They are located within the fluvial-marine transition (FMT) and are accumulations of sedimentary deposits (mouth bars, levees, wetlands, inter-distributary bays) resulting from sediment delivered by rivers via a network of distributary channels. Deltas are highly productive ecosystems that serve as centers for human population, harbor fisheries, support agriculture, and provide corridors for commerce. Delta's worldwide are threatened by environmental change including high rates of subsidence (Dokka., 2006; Törnqvist et al., 2008), global sea level rise (Donnelly et a., 2004; Church and White., 2006), reduced sediment inputs (Blum and Roberts, 2009; 2012; Giosan et al., 2014), altered nutrient budgets (Turner, 1997; Day et al., 2007), and a suite of other local factors (Syvitski and Saito, 2007). The Mississippi River Delta (MRD) typifies these impacts with recorded land loss of over 4,800 km² in the past century, threatening the population, infrastructure, and reducing ecosystem services (Day et al., 2007; Couvillion et al., 2011).

To combat land loss in the MRD, numerous groups have advocated for partially diverting the flow of the Mississippi River to reinitiate the natural processes that originally built this delta (Gagliano and van Beek, 1975; Day et al., 2007; Kim et al., 2009; Allison and Meselhe, 2010; Paola et al., 2011; Edmonds, 2012; LACPRA, 2012). This idea that was first suggested by Sherwood Gagliano in the 1970s, and was endorsed by the scientific community, as well as adopted by the State of Louisiana's 2012 and 2017 Coastal Master Plan for Coastal Restoration

(Gagliano and van Beek, 1975; Day et al., 2007; Kim et al., 2009; Allison and Meselhe, 2010; Paola et al., 2011; LACPRA, 2012). While economically an efficient way to build land in the MRD (Kim et al., 2009; LACPRA, 2012), there are too few analogs aside from laboratory studies (e.g. Hoyal and Sheets, 2009; Straub et al., 2015, Li et al., 2016), numerical modeling studies (Edmonds and Slingerland, 2007; Hanegan, 2011; Caldwell and Edmonds, 2014), theoretical and geometric approaches (Kim et al., 2009; Paola et al., 2011), reduced complexity models (Liang et al., 2015; Liang et al., 2016) and limited field observations (Paola et al., 2011; Clark, et al., 2013; Esposito et al., 2013; Shaw et al., 2013).

Wright and Coleman (1974) describe river mouth bar development in relationship to a turbulent jet-plume. The turbulent jet-plume flows into standing water, friction causes deceleration, flow expands and sediment deposits. Wright (1977) suggested that mouth bar formation is governed by three effluent forces; outflow inertia, turbulent bed friction seaward of the mouth, and outflow buoyancy, when neglecting modification by tides or waves. Each force depends on discharge (water and sediment), outflow velocity, water depths (in and seaward of the river mouth), grainsize, and density contrasts between the river and basin waters. Outflow densities are defined as homopycnal (outflow density is the same as basin water density), hypopycnal (outflow is buoyant) and hyperpycnal (outflow is denser than basin water) (Bates, 1953). The work of Wright and Coleman (1974) and Wright (1977) was furthered by Edmonds and Slingerland (2007) who used several non-dimensional metrics to determine the mechanics governing the formation and evolution of river mouth bars in river-dominated deltas. They supplemented their theoretical approach with numerical modeling, to support the development of a non-dimensional metric to estimate the position of the mouth bar (Eq. 1; Eq. 2) within a delta channel network. Assuming river-dominated conditions apply Eq. 2 can be re-arranged into a

non-dimensional form (Eq. 1), where the distance to the mouth bar L_{RMB} is divided by the average depth of that channel segment. The reduced right-hand side (RHS) of Eq. 3, namely jet momentum flux (JMF) is presented as a proxy for the required fluid inertia forces needed to mobilize and transport sediment grains, and scales linearly with the non-dimensional distance to the mouth bar. Hence, the dimensionless distance to the mouth bar can be computed using:

$$\frac{L_{RMB}}{D} = 104 \left[\frac{\rho W U^2}{(\sigma - \rho) g D_{50} W_{max}} \right]^{0.2278} \quad (1)$$

Where, the distance to the mouth bar can be found by recasting the above equation in the form below:

$$L_{RMB} = 104 \left(\frac{D_o}{2^{kn}} \right) \left[\frac{\rho}{(\sigma - \rho)} \frac{W_o}{2^{bn}} \frac{U_o^2}{2^{2mn}} \frac{1}{W_{max}} \right]^{0.2278} \quad (2)$$

and JMF can be approximated using the following equation:

$$\frac{\rho W U^2}{(\sigma - \rho) g D_{50} W_{max}} \quad (3)$$

where L_{RMB} is the distance to river mouth bar, W is the average bifurcation width leading to the mouth bar, W_o is the initial (trunk channel) width, W_{max} is the max bankful width, D_o is the initial (trunk channel) channel depth, U_o is the initial velocity of zero order bifurcation, U is local velocity, g is acceleration due to gravity (9.81 m/s^2), D_{50} is the median grain size at bed, K is 0.383, m is 0.227, b is 0.39, n is the bifurcation order number, ρ is the fluid density $\sim 1,000 \text{ kg/m}^3$, and σ is the density of quartz $\sim 2,600 \text{ kg/m}^3$. Here b , K , and m are the exponents from hydraulic geometry relationship.

To assess how distributary channel geometries, change when subjected to multiple bifurcations, Edmonds and Slingerland (2007) acquired bifurcation lengths (L), widths (W), and depths (D) for the Mossy Delta, and for several other deltas including the Wax Lake outlet. They show that the average (normalized) non-dimensional bifurcation order channel length (L/W_0), width (W/W_0) and depth (D/D_0) demonstrate an exponential decay trend, decreasing with increasing bifurcation order.

In an attempt to rapidly assess delta growth dynamics in slowly evolving landscapes, Wolinsky et al. (2010) derived four delta allometry laws that govern the growth of river-dominated deltas. They used time series satellite images of a river dominated delta (the Mossy Delta) supplemented with an experimental, and a numerical. They acquire four area perimeter measurements in their study A_{land} , L_{shore} , A_{wet} , and L_{wet} . A_{land} is the area of the delta it is bounded by the seaward shoreline and initial land before delta growth, L_{shore} is the perimeter of that boundary. A_{wet} is the total area of subaerial or wetted land within the delta area, and L_{wet} is the total perimeter of the subaerial land. Wolinsky et al. (2010) suggest land area and shore perimeter in river-dominated deltas display isometric growth while delta channel pattern demonstrate fractal growth. Edmonds et al. (2011) examined delta similarities further, by introducing additional metrics of delta morphology that focused on the channel network. This approach was not new, as Fagherazzi et al. (1999) and Rinaldo et al. (1999) applied metrics derived from tributary networks to tidal delta networks and reported little scale invariance, as did Straub et al. (2007) where they found scaling similarities between submarine channel networks and tributary fluvial networks. Both Straub et al. (2007) and Edmonds et al. (2011) reported similarities of delta distributary channel networks, and submarine channel networks respectively, analogous to Hack's law for drainage basins (Hack., 1957).

Howes et al. (2012) suggested that a scaling exist for channels within the Fluvial to Marine Transition (FMT). They approached scaling of these systems using simple channel geometry parameters such as width and depth, and examined how these parameters vary across the FMT, from the marine boundary to the end of the backwater zone. They document that channels within the FMT exhibit a proportional relationship between width and depth along the entire reach of each system, and that FMT systems fall within the same parameter space as fluvial and submarine systems/channels as well as tidal blind systems, suggesting scale invariance. Regardless of size, tributary, tidal, and fluvial networks exhibit similar scaling laws (Straub et al., 2007; Wolinsky et al., 2010; Edmonds et al., 2011; Howes et al., 2012).

Laboratory deltas are one way to study the processes and controls of delta formation (Hoyal and Sheets, 2009). Evolving under controlled conditions, they allow scientist to study steady states, responses to changes in a single variable, and can be measured comprehensively to a degree that is rarely possible in the field, at much shorter time scales than larger systems (Paola et al., 2011). However, most laboratory deltas fall short of being dynamic scale models (Paola et al., 2009), yet they seem to capture the essence of many important processes in natural systems (Paola et al., 2009) and compare well, despite differences of spatial scale, time scale, and material properties.

Boyer et al. (1997) described sub-delta crevasses (SDC) as land formations resulting from sediment-laden waters flowing through a break in the natural levee into an interdistributary bay or receiving basin. The receiving basins are semi-enclosed by natural levees formed from other channels surrounding the basin restricting flow to outflow channels. Once a channel forms, bifurcations take place expanding the land area (Welder, 1959). SDC resemble deltas in terms of their planform morphology and they exhibit deposits similar to larger deltas such as mouth-bars,

sub-aqueous and sub-aerial levees. The SDC in this study were constructed in cooperation with the U.S. Fish and Wildlife Service (USFWS; 83-1, 92-5, and 93-1; Figure 1) and the Coastal Protection and Restoration Authority (CPRA) as part of the Delta-wide crevasses maintenance project (MR-09; 06, 09, 11, 12, 15, 20, 31, 36, 38, 51, and OP-5; Figure 1) in the Delta National Wildlife Refuge (DNWR) in Louisiana. These constructed SDC are shallow relative to the depth in the parent channel receiving mostly suspended load. Sand is transported and deposited in the SDC at higher river stages, as the floodwater recede mud is deposited creating alternating mouth bar deposits (Esposito et al., 2013). Boyer et al. (1997), Turner and Boyer (1997) and Yocum and Georgiou (2014) evaluated growth rates of SDC and reported some basic controls governing their evolution, namely anthropogenic crevasses the investigation of Boyer et al. (1997). The growth rate of the SDC is highest after initial construction and following maintenance, diminishing exponentially with time (Yocum and Georgiou, 2014). However, not all attempts to create land as a SDC are successful.

Despite considerable advances in rapid delta and distributary channel growth/extension assessment to provide metrics for planform morphology, or to document change, the planform morphology of smaller deltas - those found at scales of much larger than laboratory, but much smaller than sub-delta - are still lacking. Much remains unknown about how these systems transport, deposit, and retain sediment. Sub-delta crevasses bridge this gap, they do not suffer from scaling laws such as laboratory deltas and they are small enough to allow for fast synoptic observations. Here we examine sub-delta crevasses in the MRD to determine if they obey delta scaling laws (Edmonds and Slingerland, 2007; Wolinsky et al., 2010; Howes et al., 2012) and identify mechanics governing sedimentation characteristics.

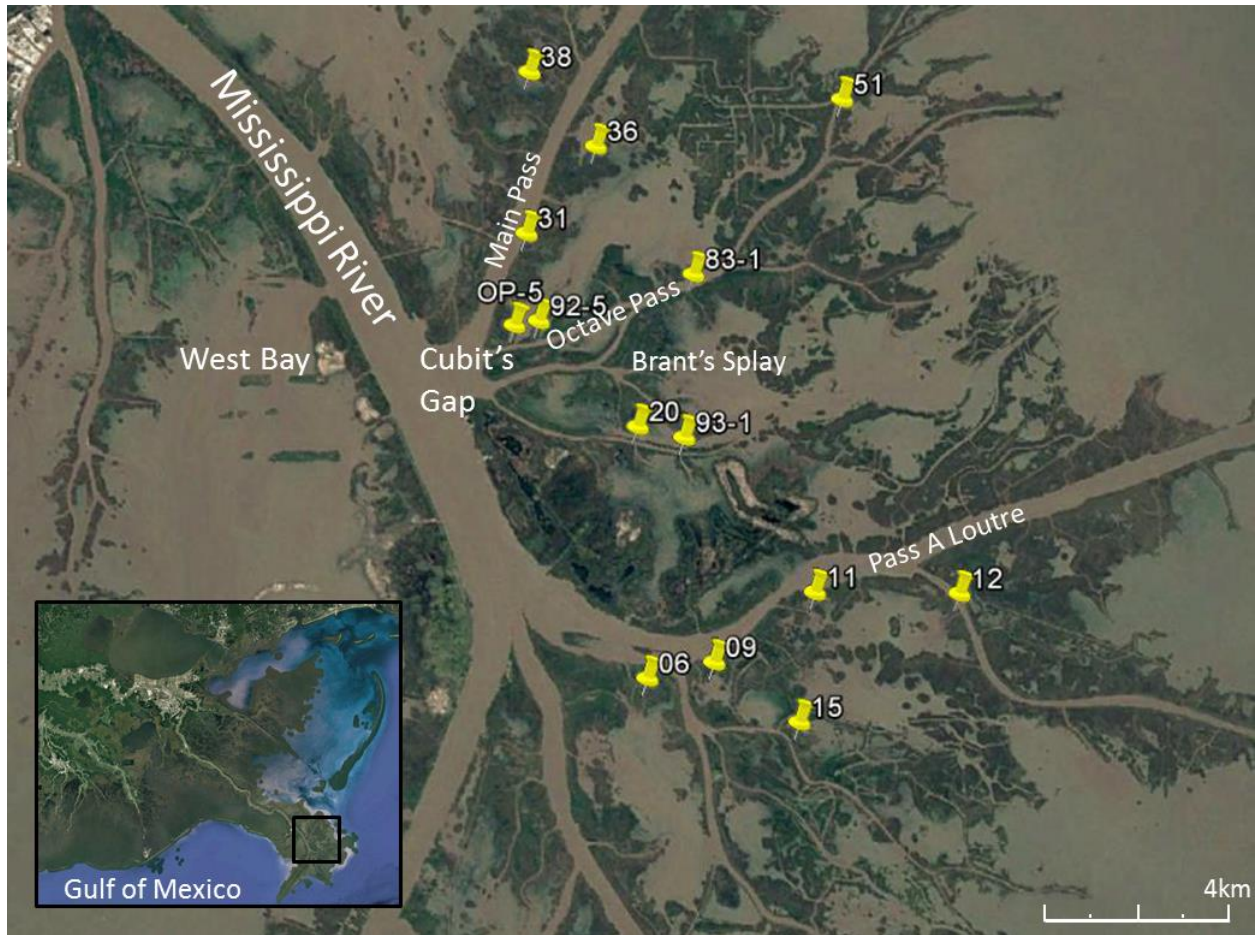


Figure 1: Map of the study area within the Mississippi River Delta, MR-09 projects (06, 09, 11, 12, 15, 20, 31, 36, 38, 51, and OP-5 UDC), USFWS projects (92-5 DC, 93-1, and 83-1), and Brant's Splay. Image from Google Earth.

Hypotheses

Deltas worldwide, sub-delta crevasses in the MRD, and experimental deltas exhibit remarkable similarities, however variations do exist (Hoyal and Sheets, 2009; Wolinsky et al., 2010; Edmonds et al., 2011; Geleynse et al., 2011; Caldwell and Edmonds, 2015). Development of sub-delta crevasses are a part of the natural processes that originally built the MRD therefore, it seems reasonable that sub-delta crevasses in the Mississippi River Delta would follow the growth laws previously mentioned. To examine sub-delta crevasse performance, metrics and controls that governing their evolution and morphological change, the following hypotheses are tested:

(H1): Sub-delta crevasses within the MRD follow the same scaling laws as large deltas. Non-dimensional channel metrics are expected to follow exponential decay relationships with respect to bifurcation order and scale linearly with jet momentum flux. Crevasse development will follow delta allometry metrics and width to depth scaling relationships.

(H2): In a sub-delta crevasse, the competency of the channel network to carry sediments is governed by the channel network and basin geometry. Depocenters will exhibit basinward migration as a function of sub-delta crevasse development. Crevasse development will exhibit asymmetric channel network growth when subjected to receiving basin characteristics (Basin depth and planform geometry).

Material and Methods

3.1 Planform Metrics and Growth Laws

To assess growth laws in deltas and compare with SDC we created a database by digitizing several large deltas from Edmonds and Slingerland (2007) and fourteen SDC in the modern Mississippi River Delta (MRD, Balize), ranging from newly constructed undeveloped sub-delta crevasse (e.g. OP-5 [UDC]; Figure 1) to fully developed (e.g. 92-5 [DC]; Figure 1). Brant's Splay, Wax Lake Delta (WLD), and Atchafalaya Delta (AD) as well as two experimental deltas (TDB_12 and 13; Figure 3) were added to the data set. Planform channel and delta metrics (length, width, wetted area, wetted perimeter, delta area, and delta perimeter) of the SDC and larger deltas were obtained using geospatial tools such as ArcGIS and Google Earth® (Figure 2, left). Channel depths were obtained from crevasse project (MR-09) data reports (CPRA), bathymetric datasets from this study, and previous works (e.g. Esposito et al., 2013) and other unpublished datasets collected by the Coastal Hydrodynamics and Sediment Transport Laboratory. Median grain diameter for the two instrumented crevasses (OP-5 and 92-5; Figure 1) was obtained using sediment grab samples. Velocities were obtained using vessel based ADCP for three of the crevasses (UDC, DC) herein including Brant's Splay. While velocities (U) for the remaining systems were estimated using subcritical Froude numbers (Fr) from gathered literature. We compiled local subcritical Froude numbers and shear velocities from synoptic ADCP at more than 50 locations in Cubit's Gap (Esposito et al., 2013) and South Pass (Clark et

al., 2013). Using the Froude numbers (0.15 to 0.22) and the local depth (D) at each bifurcation location we determine the local velocity (Eq. 4). The velocity prediction at each channel utilized a random number generator approach to select a Froude number from observations (Clark et al., 2013; Esposito et al., 2013).

$$U = Fr\sqrt{gD} \quad (4)$$

Delta allometry followed methodology detained in Wolinsky et al. (2010) which includes the channel network wetted perimeter (L_{wet}) and area (A_{wet}), sub-areal delta land (A_{land}) and delta perimeter (L_{shore}) (Figure 2, right). Areas and perimeters were extracted from Google Earth Pro® for six SDC (12, 20, 51, the DC [92-5], 93.1, and 83.1; Figure 1) and were repeated on three to five different dates depending on image quality and availability.



Figure 2: Bifurcation widths and lengths to bifurcation order (left). The developed crevasse (92-5) delta allometry metrics from Wolinsky et. al. (2010; right). Images from Google Earth.

We incorporated planform metrics for two experimental deltas from the Sediment Dynamics Laboratory at Tulane Universities Department of Earth and Environmental Sciences (Figure 3). Both experimental deltas have the same sediment size distribution (range from 1 to

1,000 μm , mean 67 μm), sediment discharge ($3.91 \cdot 10^{-4}$ kg/s), water input ($1.72 \cdot 10^{-4}$ m³/s), sea level rise (0.25mm/h), and no tidal fluctuation. The only difference between the experiments was the amount of polymer added, which controls sediment cohesion. Experiment TDB-13 (Figure 3, right) was weakly cohesive having 40g of polymer per 54kg of sediment, about half the polymer as TDB-12 (Figure 3, left), which was strongly cohesive having 80g of polymer per 54kg of sediment (Straub et al., 2015). Channel and delta metrics were assessed using topographic scans made every hour with a 3-D LiDAR scanner, image analysis using RGB values obtained throughout the experiment every fifteen minutes, taking into consideration sea level rise. Image capture included a dye in the water to highlight the channel network. Channel length and width, and delta area and perimeter information were derived using image analysis, while channel depths utilized the LiDAR. This analysis was repeated every 20 hours (experiment time) for a total of 20 to 45 observations (delta snapshots) for the duration of the experiment, unless the delta was reorganizing at which point the observation was omitted.

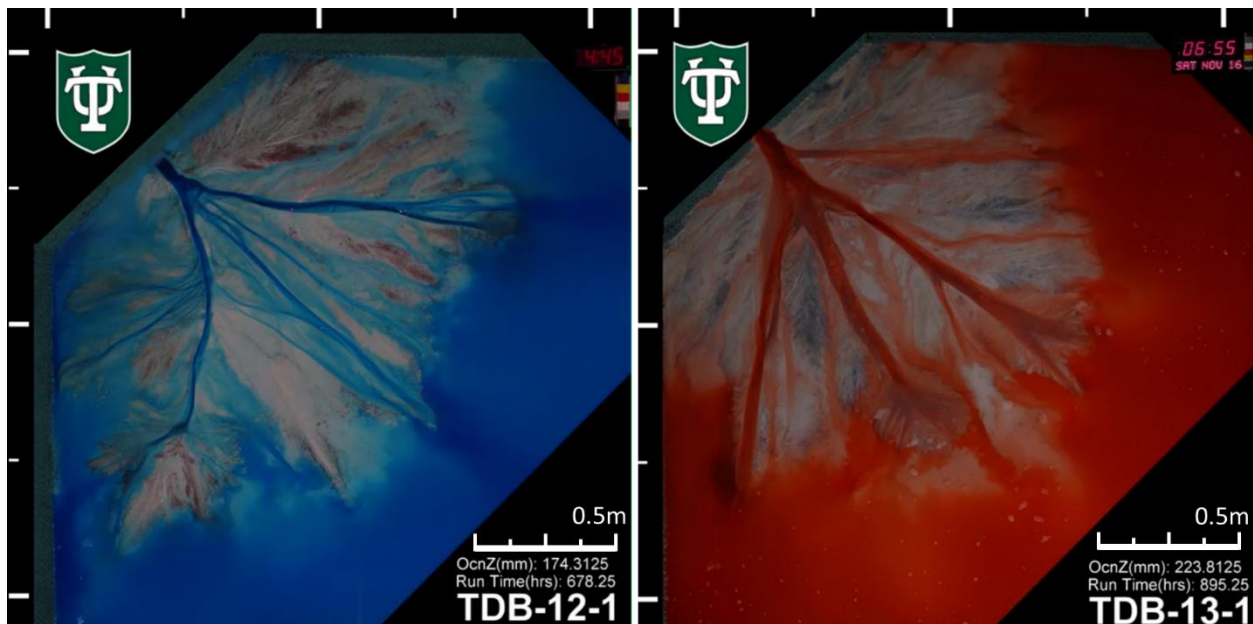


Figure 3: Experimental deltas from Tulane Universities Department of Earth and Environmental Sciences Sediment Dynamics Laboratory. (Left) Experiment TDB-12 (Right) and TDB-13 (Straub et al., 2015).

3.2 Field Data Collection

To obtain water and sediment fluxes through the crevasses, establish flow distribution through proximal channels and reference concentrations of suspended sediment concentration (SSC) during floods, we deployed tripods that employed hydro-acoustic sensors, conducted vessel based synoptic ADCP surveys, and collected sediment samples using a petit ponar throughout the channel network and crevasse receiving basin (i.e. surface water samples, grab samples, and cores). Instrument deployments provided current profiles and water level at the entrance to the undeveloped (UDC; OP-5) and developed sub-delta crevasses (DC; 92-5). We used vessel based synoptic ADCP surveys to determine the current profiles (and discharge) across Cubit's Gap (entrance to sub-delta; Figure 4A), multiple locations across Octave Pass (main distributary leading to the sub-delta crevasses of interest; Figure 4A), and at the entrances of both the UDC and DC. Sediment samples were collected to establish spatial trends in bottom sediment grainsize distribution, while water samples were collected to assess the spatial distribution of SSC within both sub-delta crevasses receiving basins, and channels leading to the crevasse entrance.

Two Nortek Aquadopp Profilers were mounted on a tripod and deployed in the main channels of the UDC and DC (Figure 4A; Aqua A and Aqua B). Flow and water level measurements were recorded at 2 Hz for five minutes, with a fifteen-minute interval between measurements. Approximately half a kilometer downstream from an Aquadopp profiler - in the DC - a RBR-TWR was deployed on a stake that was driven to refusal, and recorded average water level measurements in five-minute intervals. Instruments were deployed for thirty days from January 21st to February 19th, 2016.

Previous synoptic ADCP data from April 2015 was added to two vessel based ADCP surveys conducted on February 19th, 2016. On February 19th, the first survey began at approximately 11AM, and consisted of twelve transects. Transects were made at the entrance of Cubit's Gap, multiple locations across Octave Pass, and at the entrances of both SDC (Figure 4A). The second survey consisted of five transects beginning at approximately 4PM, at the entrances of the two SDC and at three locations across Octave Pass. Flow data collected from the ADCP surveys was used to determine how much of the main channel flow is supplied to the SDC. Flow data was additionally supplemented with data from the USACE station at Belle Chasse, LA, who performed similar observations in the main stem of the Mississippi River, and all major distributaries and outlets.

Sediment samples were collected at nineteen locations within and surrounding both SDC on February 19th, 2016 (Figure 4B). Cores were taken at eight of the nineteen locations. I used a kayak to recover the eight cores and eight of the surface water and grab samples within the UDC (Figure 4B and C). At each core location, the surface water samples were taken by hand with a 500 ml bottle before retrieving the grab and core samples so that any disturbances that may happen during the extraction of the grab sample is not reflected in the water samples. Cores were retrieved using a half meter Russian sediment/peat borer. Once recovered the cores were photographed, placed into half a PVC pipe, wrapped in plastic wrap, and taped closed for transport. The eleven remaining water and grab samples were taken from a boat using 500 ml bottle and a Petit Ponar. Samples were stored and transported in an ice chest, once at the lab they were kept refrigerated until analysis.

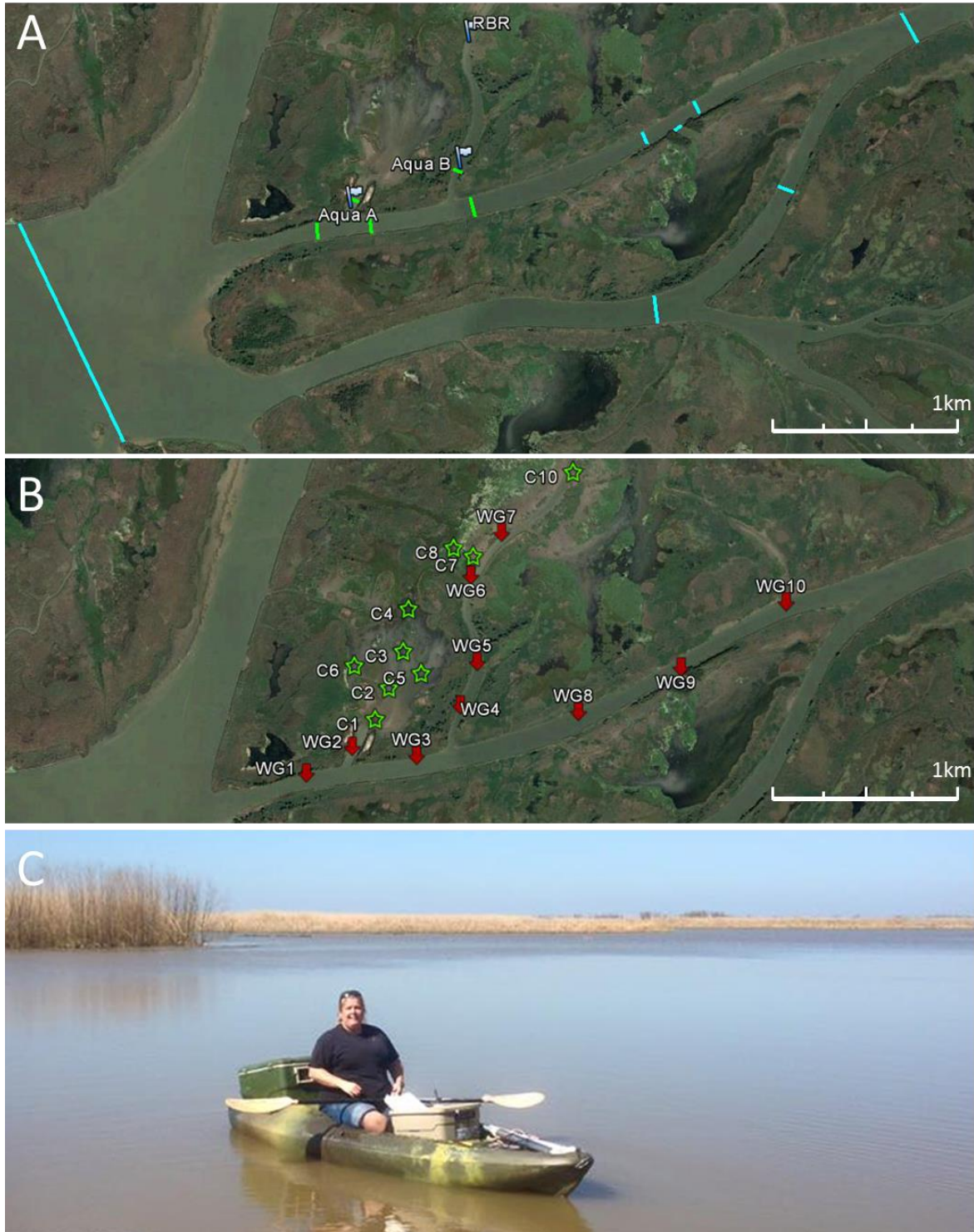


Figure 4: (A) Deployment locations of Aqua A, Aqua B, and the RBR as well as ADCP transect locations (blue and green lines). The green and blue lines indicate transects that were made at 11AM and the blue lines only indicate transects that were made at 4PM. (B) Core locations are indicated with green stars. Surface water and grab samples are indicated with red arrows and green stars. Images A and B from Google Earth. (C) Me on the kayak about to collect cores in the UDC.

3.3 Hydrodynamic Analysis

Velocities obtained from vessel based synoptic ADCP surveys were used to calculate jet momentum flux (Edmonds and Slingerland, 2007). Time depended velocity from both deployments at crevasse entrance were vector resolved to yield the streamwise and transverse component aligned with the crevasse entrance axis. Velocity profile was integrated to yield depth average velocity and produce specific discharge (q , $m^3/m/s$). Instantaneous discharge was achieved by extrapolating specific discharge across the channel entrance and utilizing the synoptic ADCP and though correlations with the USGS Belle Chasse station produced an annual discharge hydrograph for both crevasses. Crevasse water discharge was calculated by utilizing the ADCP transect profile for both the UDC and DC. Each transect profile was divided into four segments with an average depth per segment to calculate the total area. The total water discharge (Q) was calculated by distributing the measured specific discharge at the deployment location across the channel width using the depth raised to a $2/3$ power derived from the Manning's equation (Chow, 1958) for the time period of measured data. The predicted Q was adjusted to match fields observations using a coefficient of 0.8 to account for a flow contraction at the crevasse entrance. A linear regression equation was calculated between the observation window at the crevasses and the hydrograph at Belle Chasse, this was used to develop an annual discharge hydrograph for both of the crevasses. Suspended sediment discharge (Q_s) was calculated using water discharge (Q) and suspended sediment concentrations from the field (see section 3.4).

3.4 Sedimentological Analysis

To obtain a spatial distribution of sediment size, grain size analysis was performed using mechanical sieve analysis based on the method described in *Soil Sampling and Methods of Analysis* (Carter, 1993) and the ASTM hydrometer method of particle-size analysis, D 422-63 (ASTM, 2008c). GRADISTAT, a grain size distribution and statistics program for the analysis of unconsolidated sediments, was used to obtain median grain diameter and distribution. Grab samples were mechanically sieved with seven sieves from 500 microns (coarse sand) to 64 microns (very fine sand) and hydrometer analysis was performed on the fines (sediment < 64 microns) providing fractions of very course, course, medium, fine, and very fine classes of silts and clay allowing for more accurate D_{50} .

Suspended Solids Concentration was performed on the surface water samples using a method based on the *Standard Test Methods for Determining Sediment Concentration in Water Samples* (ASTM D 3977-97). Samples were syphoned through a pre-weighed 47 mm hydrophilic glass fiber filter with a 0.7 μm pore size to obtain a TSS concentration and provide an understanding of the suspended sediment concentrations throughout the study area.

3.5 Numerical Modeling

Using the 2-D version of Delft3D (a multi-dimensional physics-based morphodynamic model that can simulate flow, and sediment transport) sub-delta crevasse formation was modeled, testing H2. Delft3D solves the depth-integrated equations of motion using conservation of mass and momentum principles (Lesser et al., 1994, Deltares, 2015). Suspended sediment transport is calculated by solving the three-dimensional advection-diffusion equation:

$$\frac{\partial c_i}{\partial t} + \frac{\partial u_x c_i}{\partial x} + \frac{\partial u_y c_i}{\partial y} + \frac{\partial (u_z - w_{s,i}) c_i}{\partial z} = \frac{\partial}{\partial x} \left(\varepsilon_{s,x,i} \frac{\partial c_i}{\partial x} \right) + \frac{\partial}{\partial y} \left(\varepsilon_{s,y,i} \frac{\partial c_i}{\partial y} \right) + \frac{\partial}{\partial z} \left(\varepsilon_{s,z,i} \frac{\partial c_i}{\partial z} \right) \quad (5)$$

where c_i is mass concentration of the sediment fraction (kg/m^3), assumes a standard Rouse profile concentration gradient, u_x , u_y , and u_z , are the directed fluid velocities (m/s), $w_{s,i}$ is the setting velocity of the sediment fraction (m/s), $\epsilon_{s,x,i}$, $\epsilon_{s,y,i}$, and $\epsilon_{s,z,i}$ are directional eddy diffusivities of the sediment fraction (m^2/s). Settling velocities are set according to Stokes' law for cohesive sediments, ignoring flocculation effects and to Van Rijn (1993) for noncohesive sediments depending on the grain diameter:

$$w_{s,i} = \begin{cases} \frac{RgD_i^2}{18\nu}, & 64 \mu\text{m} < D_i < 100 \mu\text{m} \\ \frac{10\nu}{D_i} \left(\sqrt{1 + \frac{0.01RgD_i^3}{\nu^2}} - 1 \right), & 100\mu\text{m} < D_i < 1000\mu\text{m} \\ 1.1\sqrt{RgD_i}, & 1000\mu\text{m} < D_i \end{cases} \quad (6)$$

where R is the submerged specific gravity ($\rho_s/\rho_w - 1$), ρ_s is the specific density of sediment (kg/m^3), ρ_w is the specific density of water (kg/m^3), g is the acceleration due to gravity (9.81m/s^2), D_i is the grain size diameter of the sediment fraction (m), and ν is the kinematic viscosity coefficient of water (m^2/s). Noncohesive suspended sediment exchange with the bed is calculated as an erosive flux due to upward diffusion and a depositional flux due to sediment settling. Cohesive sediment erosion and deposition is calculated using the Partheniades-Krone formations (Partheniades, 1965):

$$F_{e,i} = \begin{cases} \left(\frac{\tau_0}{\tau_{ce(C)}} - 1 \right), & \text{when } \tau_0 > \tau_{ce(C)} \\ 0, & \text{when } \tau_0 \leq \tau_{ce(C)} \end{cases} \quad (7)$$

$$F_{d,i} = W_{s,i} c_{b,i} \begin{cases} \left(\frac{\tau_0}{\tau_{cd(C)}} - 1 \right), & \text{when } \tau_0 < \tau_{cd(C)} \\ 0, & \text{when } \tau_0 \geq \tau_{cd(C)} \end{cases}$$

where $F_{e,i}$ and $F_{d,i}$ are erosive and depositional fluxes of the cohesive sediment fraction ($\text{kg}/\text{m}^2/\text{s}$), τ_o is the bed shear stress (N/m^2), $\tau_{ce(C)}$ and $\tau_{cd(C)}$ are critical shear stresses for erosion and deposition of the cohesive sediment, and $c_{b,i}$ is the sediment concentration near the bed of the sediment fraction (kg/m^3). The bed level is then adjusted accordingly with source and sink terms. Bedload transport is calculated using Van Rijn (1993):

$$q_{b,i} = 0.006w_{s,i}D_i \left(\frac{u(u-u_{c,i})^{1.4}}{(RgD_i)^{1.2}} \right) \quad (8)$$

where $q_{b,i}$ is the bedload sediment discharge per unit of the sediment fraction (m^2/s), u is the depth averaged velocity (m/s), and $u_{c,i}$ is the critical depth averaged velocity (m/s) for initiation of motion of the sediment fraction. Direction of the bedload transport is determined by local flow conditions and adjusted for bed-slope effects (Bagnold, 1966; Ikeda, 1982).

3.5.1 Model Grid and Basin Design

For this study a curvilinear grid was developed in the Deltaries GUI was used to avoid stair stepping in the channels. Stair stepping usually happens when the modeler tries to cover some area where the boundary does to follow the Orthogonality of the grid. The grid was approximately 2,245 m wide and 3,835 m long and was run in depth average mode. We used three basin types (study site, full boundary, and half boundary). The study site basin (SS) was modeled after the study site location, so the model could be calibrated according to field measurements, and to test the planform geometry aspect of H2. This basin had two SDC (UDC and DC) with land boundaries surrounding the sides of the grid and a full downstream water level boundary. The full and half boundary basins (FB and HB) were both open basins with no land boundaries on the sides on the grid. The only difference being a full downstream water level

boundary (FB) and a half downstream boundary (HB; Figure 5). Simulating an open receiving basin without restricted outflow and one with restricted outflow. Crevasse entrance dimensions were created from field data and imagery. The model was validated using flow and water level observations.

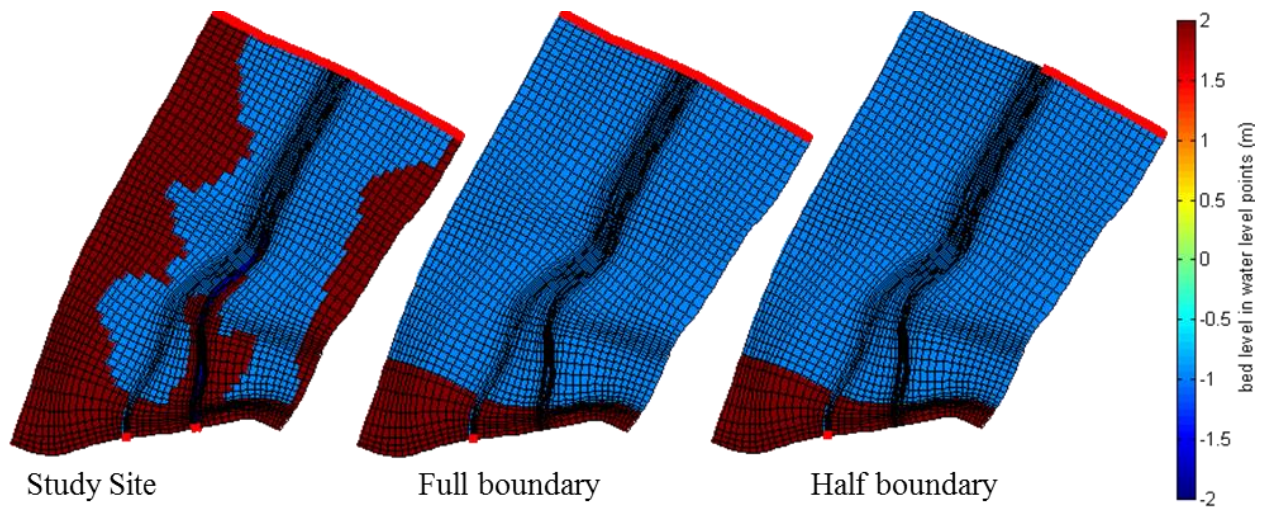


Figure 5: Model grid (black lines), basin design and boundaries (red lines) for the SS, FB and HB.

3.5.2 Initial and Boundary Conditions

All simulations started from rest and depending on the experimental design boundary conditions were either constant or varied in time. Sediment concentrations and upstream discharge (Q_s , Q) are defined using field observations in the crevasse entrance and the sand content was derived from literature (Snedden et al., 2007 and Meselhe et al., 2012). Measured SSC concentrations during flood were approximately 130 mg/l (this study), while mean annual SSC concentrations of 75 mg/l were reported by Snedden et al. (2007). Simulations with different sand content were carried out using 20% to represent flood conditions (Meselhe et al., 2012) and 5% to represent characteristic flow conditions. Three classes of sediment were used:

sand, silt and clay with the following fractions (a) 20% sand, 50% silt, 30% clay and (b) 5% sand, 60% silt, 35% clay. The sand was non-cohesive with a $D_{50} = 125\mu\text{m}$. Silt was cohesive with fresh settling velocity of 0.2mm/s. Clay was also cohesive with fresh settling velocity of 0.1mm/s. Settling velocities were chosen accordingly using Stokes Law (Stokes, 1851).

Upstream discharge varied as a function of basin geometry (e.g. SS, FB, or HB) and was either constant or varied with time. For the SS, we used a constant Q of $67 \text{ m}^3/\text{s}$ (21 and 46; two channels), and for the FB and HB a constant Q $67 \text{ m}^3/\text{s}$ (one channel). These flows represent the annual average discharge from the predicted annual hydrograph referenced in the hydrodynamic analyses (see section 3.3). Time dependent upstream discharge utilized the instantaneous annual hydrograph directly (see section 3.3).

Fluctuating water level were achieved by using tidal constituents K1(0.12m, 319deg.), O1(0.11m, 315.3deg.), P1(0.04m, 321.6deg.), Q1(0.02m, 311.7deg.), M2(0.01m, 349.7deg.), and S2(0.01m, 328.8deg.) obtained from NOAA Pilottown, LA station.

3.5.3 Model experimental design

Scenarios consisted of combinations of constant or fluctuating discharge (Q_c , Q_v), constant or fluctuating water level (WL_c , WL_v), SSC (130, 100, or 75 mg/l), sand fraction (5 or 20%), and depth variations (1m, 1.5m, 2m) rendering in 144 total simulations (Table 1; Appendix A). Simulations were set up for 60 days with a morphological scale factor of 10, simulating approximately one year and eight months (1 year, 235 days). Modeling different scenarios was intended to investigate how changes in sediment characteristics, basin geometry and water level affect sedimentation patterns, thus delta development. To assess sediment retention/channel competency as a function of the developing delta, we ran 15 day simulations

on three previously ran scenarios. Using the delta morphologies, at the end (established delta) and half-way (semi-established) points of the simulations.

Table 1: Combinations of SSC, depth, discharge sand fraction and water level using in the simulations.

Basin	SSC (mg/l)	Depth (m)	Q	Sand	Silt	Clay	Water Level
Study Site (SS)	75, 100, 130	1, 1.5, 2	Q _c , Q _~	5%, 20%	60%, 50%	35%, 30%	WL _c , WL _~
Full Boundary (FB)	75, 100, 130	1, 1.5, 2	Q _c , Q _~	5%, 20%	60%, 50%	35%, 30%	WL _c , WL _~
Half Boundary (HB)	75, 100, 130	1, 1.5, 2	Q _c , Q _~	5%, 20%	60%, 50%	35%, 30%	WL _c , WL _~

Results

4.1 Planform

Non-dimensional distance to river mouth bar (L/D) of the SDC, Brant's Splay, WLD, AD, and both of the experimental deltas (TDB_12 and TDB_13) was longer with respect to JMF than what was previously reported in larger deltas (Edmonds and Slingerland, 2007; green circles, open red circles; Figure 6). For the SDC, the WLD and experimental deltas, L/D and JMF ranged within two log cycles, while for Brant's Splay and the AD are within one (Figure 6A). Average non-dimensional channel width (W/W_o), depth (D/D_o), and length (L/W_o) decreases exponentially with increased bifurcation order, consistent with previous observations. All non-dimensional channel metrics for SDC decrease more rapidly per bifurcation order compared to large deltas from Edmonds and Slingerland (2007), while the experimental deltas channel metrics appear to decay more rapidly than the crevasses (Figure 6B, C), with the exception of L/W_o where the laboratory deltas exhibited similar response to the SDC (Figure 6D).

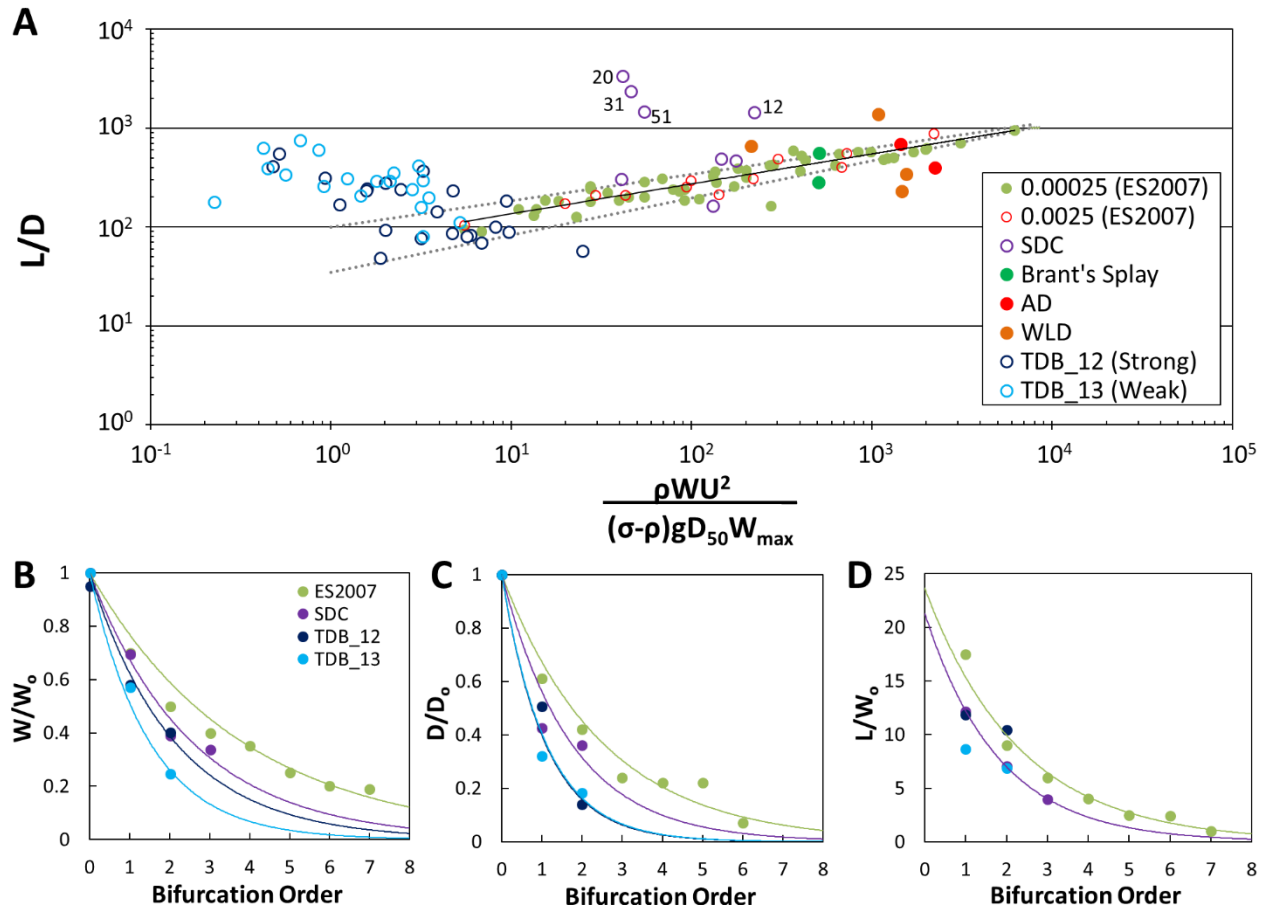


Figure 6: (A) Non-dimensional distance to the river mouth bar (L/D) to JMF. Light green, open red circles and black power trend were digitized from Edmonds and Slingerland (2007) with measured data from SDC (open purple), Brant's Splay (solid dark green), AD (solid red), WLD (solid orange), TDB_12 (dark blue), and TDB_13 (light blue). Dotted gray lines represent 80% confidence. Non-dimensional channel geometries width (B), depth (C), and length (D) for Edmonds and Slingerland (2007) deltas (green), SDC (purple), TDB_12 (dark blue), and TDB_13 (light blue) as a function of bifurcation order with exponential trends.

4.2 Delta Allometry

Delta allometry metrics presented in Wolinsky et al. (2010) test H1 further. SDC Non-dimensional land area (A_{land}/A_{max}) gradually increases with time, close to the isometric growth line (Figure 7A). Similar to Wolinsky et al. (2010) deltas, the SDC do not maintain a constant shape through time, yet the evolution of A_{land} relative to L_{shore} also exhibits almost linear growth (Figure 7B). The scaling of wetted delta area with delta perimeter (L_{wet} , A_{wet}) is substantially

different between individual crevasses and shows large variance, with some systems above, below or on the isometric growth line (Figure 7C).

Delta allometry metrics developed for the experimental deltas show a departure from other datasets. Non-dimensional land area ($A_{\text{land}}/A_{\text{max}}$) for the experimental deltas is consistently high ranging from 0.8 to 1 though the experiment (Figure 7D), while non-dimensional land area to perimeter ($A_{\text{land}}, L_{\text{shore}}$) fluctuates between 0.8 to 1 (A_{land}) and 0.6 to 1 (L_{shore}) (Figure 7E), and wetted area to perimeter ($L_{\text{wet}}, A_{\text{wet}}$) ranges from 0.4 to 1 (L_{wet}) (Figure 7F). This response can be explained as a first order by the fact that the developing delta was omitted, and only the developed delta was analyzed.

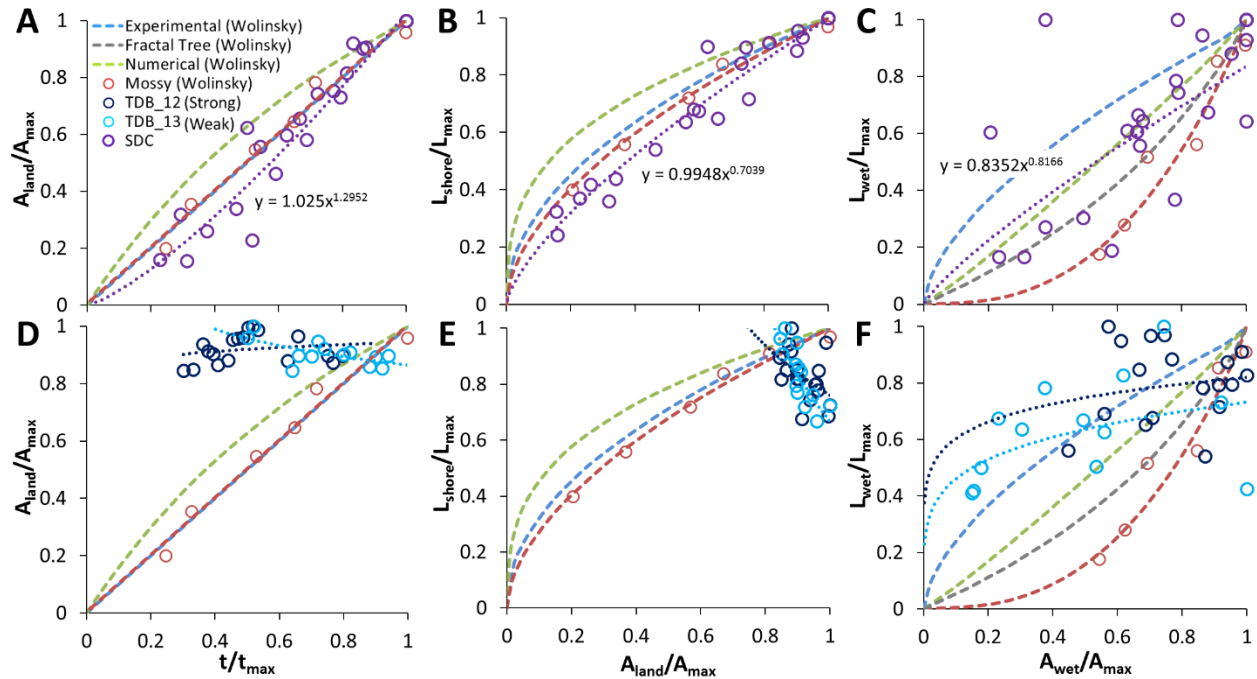


Figure 7: Delta allometry digitized from Wolinsky et al. (2010) (blue, gray, and green dashed lines and red circles). (A-C) Delta allometry for six SDC (purple), and (D-F) TDB_12 (dark blue), and TDB_13 (light blue).

4.3 Width Depth Ratio

A width depth relationship for fluvial dominated systems worldwide by Howes et al. (2012) revealed a strong linear trend. Metrics from the SDC, Brant's splay, WLD, AD and experimental deltas were added to examine if they plot within the same parameter space. SDC, Brant's splay, WLD, and AD show a similar response to other fluvial dominated systems and are within the same parameter space. SDC and Brant's Splay are between 10:1 and 100:1 ratio lines, while the AD and WLD are closer to the 100:1 ratio line. The experimental deltas, as expected, plot much lower compared to other deltas, since they are much smaller systems, and fall along ratios of 10:1 (Figure 8).

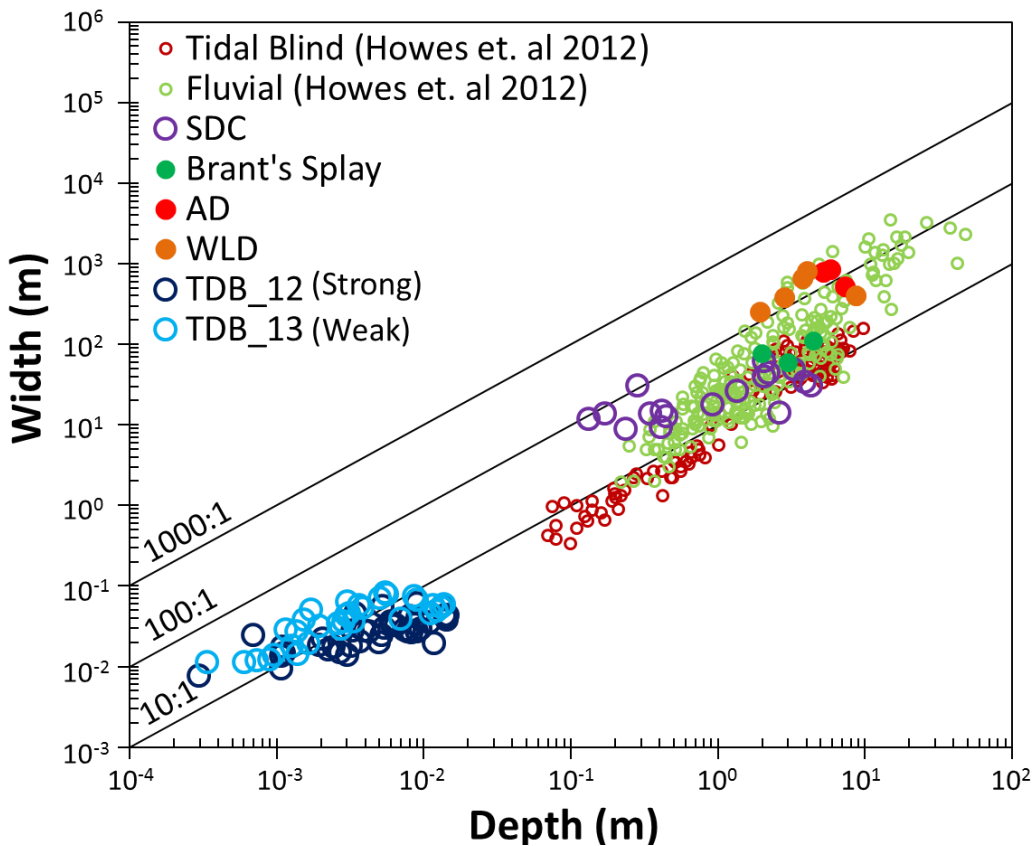


Figure 8: Width depth relationship digitized from Howes et al. (2012) (dark red and light green circles) with SDC (purple), Brant's Splay (dark green), AD (light red), WLD (orange), TDB_12 (dark blue), and TDB_13 (light blue).

4.4 Hydrodynamic

Tidal influence was documented within the channels of the UDC and DC during the 30-day deployment. Data collected reveal a tidal range between 5 cm during neap tides and 20 cm during spring tides in both the UDC (Aquapro A) and DC (Aquapro B; Figure 9). The measured tidal signal is supplemented with three tide gauges, upstream (Pilottown, NOAA), within the receiving basin (CRMS 4448) and downstream (CRMS 4626) of the UDC and DC. To quantify a relationship between water levels upstream, downstream and within the receiving basin a correlation coefficient is calculated. The correlation between the measured tidal signal and tide stations range from 0.55 to 0.84, with the highest being between RBR and Pilottown station.

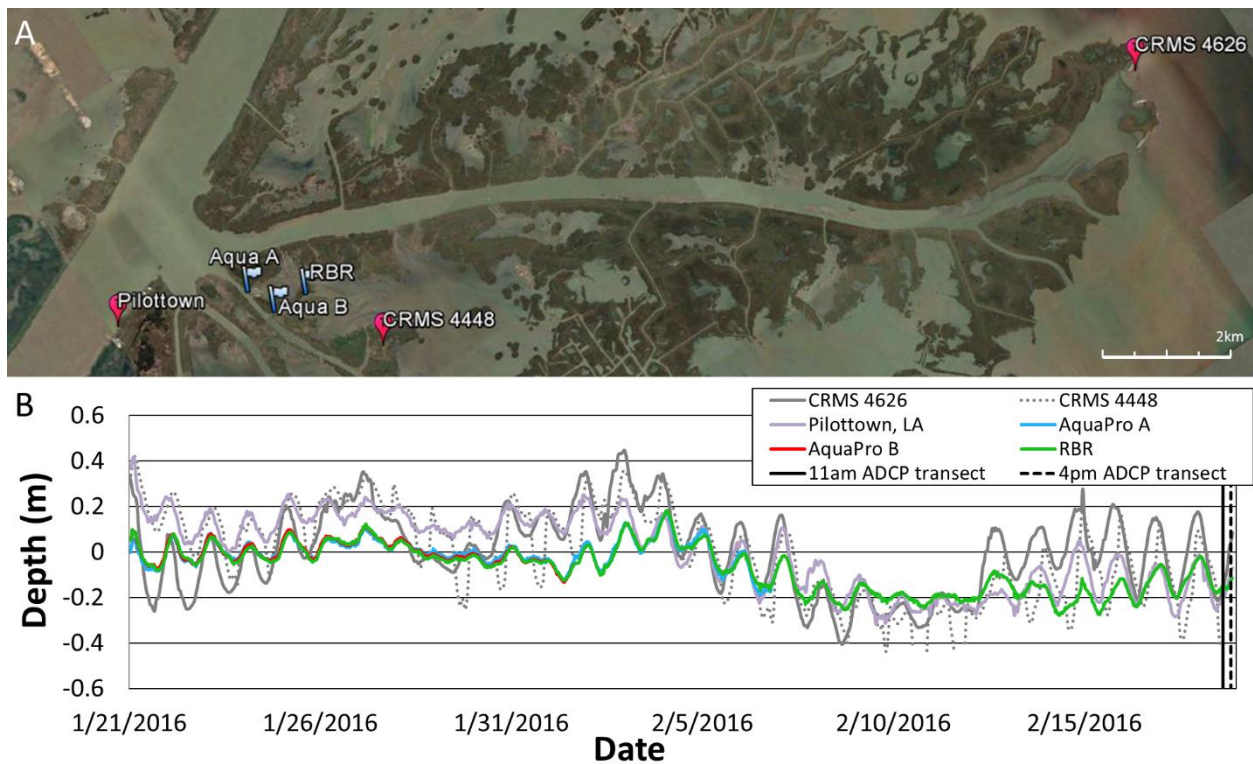


Figure 9: (A) Location of tide gauges and deployment locations. (B) Tide (m) within UDC and DC; AquaPro A (blue line) AquaPro B (red line) and RBR (green line). Tide gauge data from Pilottown (purple), CRMS4448 (dotted gray) and CRMS4626 (solid gray). Image from Google Earth.

During flood conditions on April 2, 2015, Octave Pass Q was 275 m³/s, the UDC was 17 m³/s, and 55 m³/s in the DC (Figure 10A). On February 19, 2016, Q was measured during a rising tide. From 11am to 4pm the water level in the crevasses increased by 4 cm (Figure 10D). During the same time Q into Octave pass increased from 211 to 249 m³/s, from 12 to 21 m³/s in the UDC, and from 33 to 49 m³/s in the DC (Figure 10B-C). An average of 6% of the total Octave Pass Q went into the UDC, 18% went into the DC.

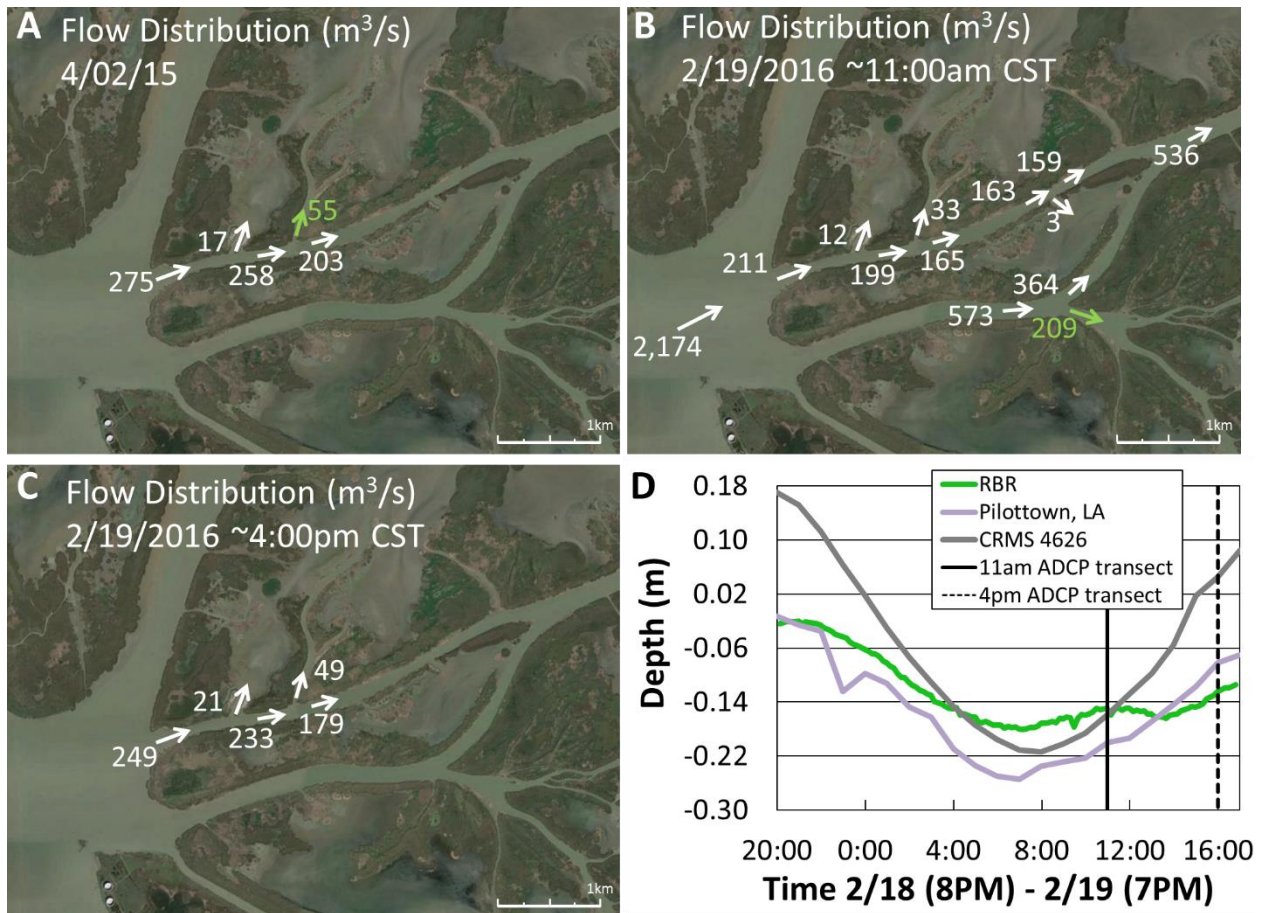


Figure 10: (A-C) Flow (m³/s) distribution on April 2, 2015, and on February 19, 2016 (~11am and 4pm). Blue arrows indicate measured flows while green is calculated by the difference in flow upstream and downstream of the location. (D) Water levels from the RBR (green), CRMS 4626 (gray) and NOAA Pilottown, LA (purple) on February 18th to February 19th. ADCP transects began at 11AM (solid black line), and ended after 4PM (dashed black line). Images from Google Earth.

During the time of the deployment discharge into the UDC and DC fluctuated with a declining trend (similar to the tidal signal). The Q went from 50 to 13 m³/s in the UDC with a maximum range of 17 m³/s and a minimum of 6 m³/s. The DC discharge went from 66 to 41 m³/s during the observation window and had a range of 15 to 6 m³/s. The extrapolated annual instantaneous discharge in the UDC was 21 m³/s. Discharge dropped to as low as 9 m³/s and rose as high as 52 m³/s. The DC had an average discharge of 46 m³/s, minimum of 37 m³/s and a maximum of 67 m³/s (Figure 11).

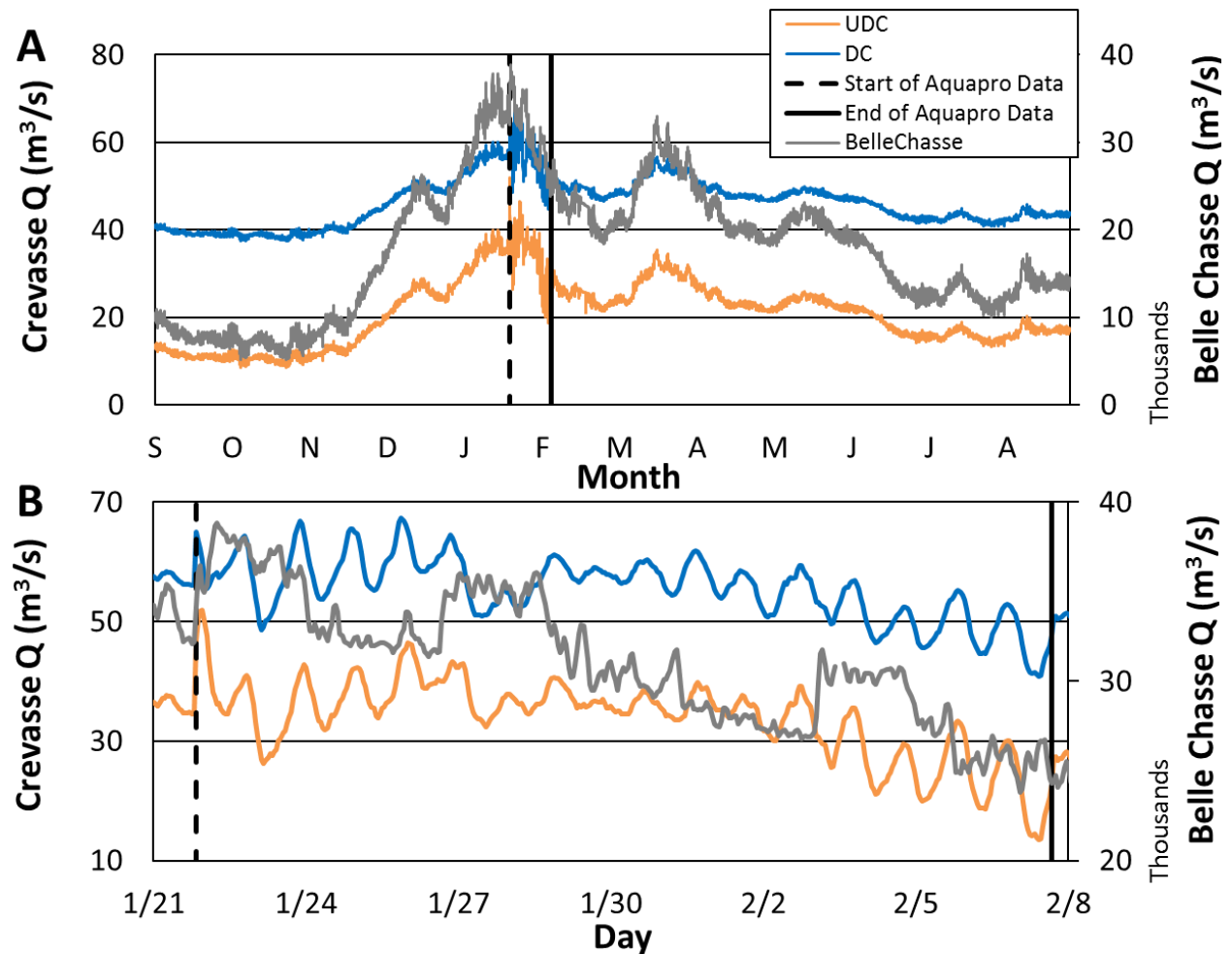


Figure 11: (A) Discharge from Belle Chasse, LA in thousands of m³/s (gray) with the extrapolated discharge for the UDC (orange) and DC (blue) in m³/s. The dashed and solid black lines are the start and end times of measured data from deployments. (B) The UDC (orange) and DC (blue) discharge during the time of the deployment window with the Belle Chasse discharge (gray).

4.5 Sedimentological

Octave Pass (Figure 1) had little variation in SSC (121 to 138 mg/l; Figure 12A). The highest concentration was approximately one kilometer basinward from the entrance to the DC (176 mg/l), where a portion of flow passed over a natural levee to the west of the main channel (Figure 12A). At the entrance of the UDC, SSC was similar to Octave Pass (120 mg/l), then decreased immediately after the crevasse entrance to 61 mg/l. SSC increased again to 122 mg/l mid-way through the receiving basin, before systematically decreasing further into the crevasse where we measured the lowest concentration in the study area (53 mg/l; Figure 12A).

Median grain size (D_{50}) obtained from bottom grab samples ranged from very fine sand to clay sized particles. Sites within the undeveloped crevasse had D_{50} between $6\mu\text{m}$ and $18\mu\text{m}$ (silt), with one exception where the D_{50} was $78\mu\text{m}$ (very fine sand). Within the main channel of the developed crevasse (from south to north) D_{50} ranged from $3\mu\text{m}$ (clay) to $90\mu\text{m}$ (very fine sand), $26\mu\text{m}$ (silt), $3\mu\text{m}$ (clay), and $16\mu\text{m}$ (silt). Along Octave Pass (from west to east) the D_{50} increases from $3\mu\text{m}$ (clay) at the beginning of the Pass to $125\mu\text{m}$ (very fine sand) just before merging with Brant Bayou (Figure 12B).

Suspended sediment discharge (Q_s) into the UDC and DC fluctuated with a declining trend from January 21, 2016 to February 8, 2016 (Figure 12E). The Q_s in the DC was about a 30 kg/s higher than the UDC during the observation period. In the DC, Q_s went from 0.0086 kg/s to 0.0053 kg/s, the UDC went from 0.0065 kg/s to 0.0017 kg/s. The maximum (0.0021 kg/s) and minimum (0.0005 kg/s) ranges were the same for both crevasses.

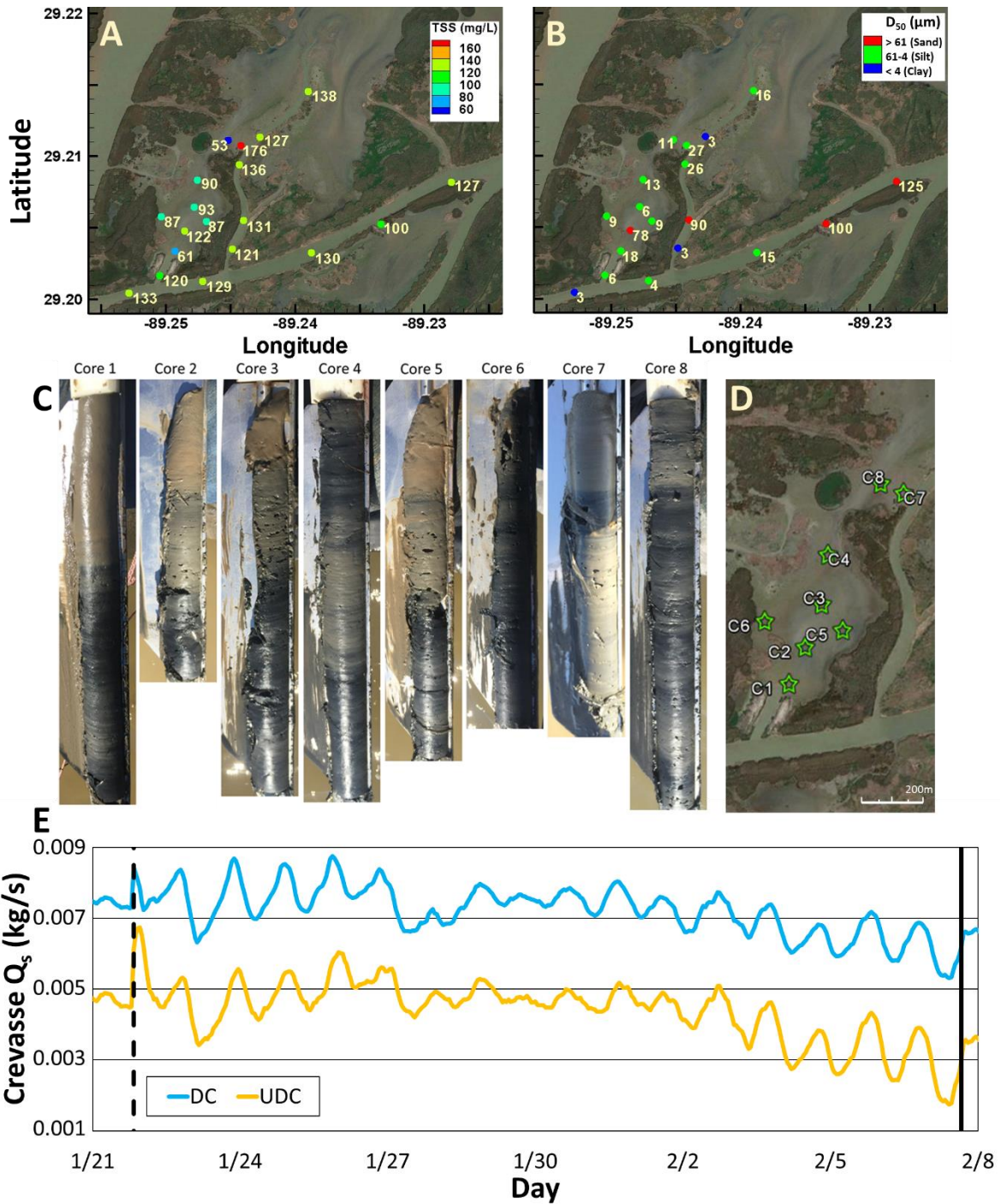


Figure 12: Results from sediment analysis. (A) Total SSC (mg/L) throughout the developed and undeveloped sub-delta crevasse and along Octave Pass. Blues represent lower concentrations with higher concentrations represented in red. (B) D_{50} (μm) throughout the DC and UDC and along Octave Pass. Sand sized material (red, greater than 61 μm), silt (green, 61 μm to 4 μm), and clay sized material (blue, less than 4 μm). (C) Photographs of cores and (D) their locations within the undeveloped crevasse. (E) Sand (dotted lines, secondary y-axis) and mud (solid lines, primary y-axis) discharge into the DC (blue) and UDC (orange) in kg/s during the deployment window (dashed and solid black lines). Images from Google Earth.

4.6 Depositional Mechanics

The model results are used to further test what controls the competency of the channel network to carry sediments. To test the effect of accommodation depth on the shape and extent of the depocenter down basin (hypothesis 2), we plotted the laterally integrated sediment volume along a centerline of the receiving basin for simulations with Q_c and WL_c for three selected depths, 1m, 1.5m, and 2m. By using Q_c and WL_c within the same basin we isolate the effect of accommodate depth as the only factor contributing to depocenter changes (Figure 13A). With increasing accommodation depth, the distance over which sediment deposition occurs shortens and the sediment thickness lowers. Sediment deposition extends outside the downstream boundary (over 3,200m) basinward of the crevasse entrance in the 1m basin, while in the 2m basin most sedimentation occurs before 2,000m and the deposit begins to thin basinward. This behavior is also reflected in the other basin types (FB, and HB; Figure 14A and B).

To evaluate the effect of discharge and tides on deposition centers, we plotted sediment volume by distance for the four combinations of fluctuating and constant Q_c and WL_c at 2m basin depth in the FB (Figure 13B and C). Sediment deposition extended furthest basinward when both Q_c and WL_c were constant (about 2,100m) and was nearest to the crevasses entrance when both Q_c and WL_c or just WL_c were/was fluctuating (900m). With Q_c and WL_c , deposition extended 1,400m basinward. Note that Figure 13A has two deposition centers one at 400m and the other at 1,400m this is because of the two crevasses in the SS basin. The developed crevasse deposits sediment further into the receiving basin than the undeveloped crevasse.

The effect of sediment supply or sand content entering the crevasse is obvious for most simulations (Figure 13A and B; Figure 14A and B). For instance, as sediment supply increases

the depocenter migrates basin-ward, and the thickness of the deposit grows. As expected, higher sand fractions produce fractionally thicker deposits that also extend basinward compared to simulations with lower sand content.

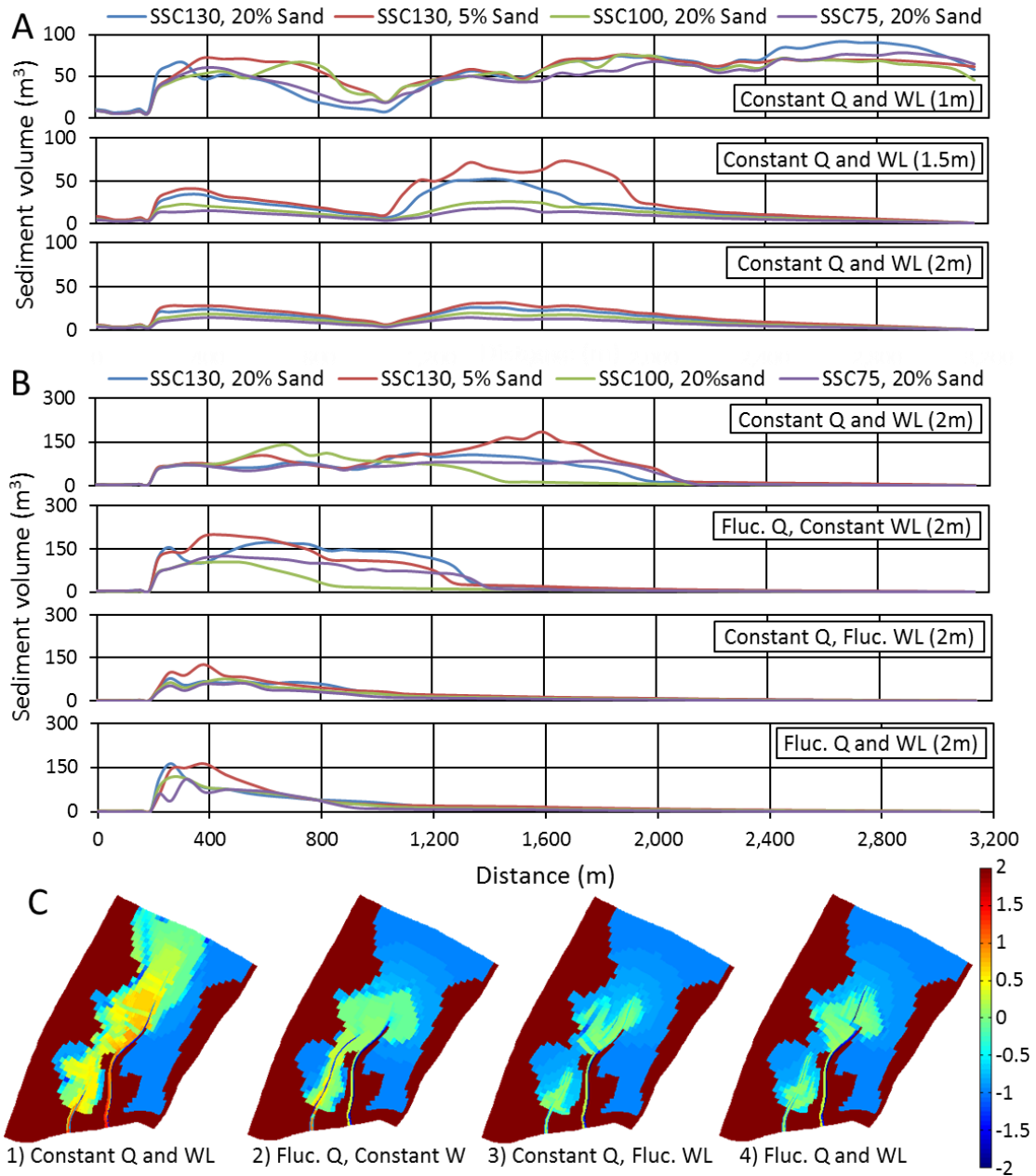


Figure 13: Relative sediment deposition volume including morph factor along the centerline of the basin for each sediment supply characteristic (SSC130, 20% sand [blue], SSC130, 5% sand [red], SSC100, 20% sand [green], SSC75, 20% sand [purple]). (A) Q_c and WL_c for each accommodation depth (1m, 1.5m, and 2m) in the SS. (B) Four scenarios 1) Q_c and WL_c , 2) Q_- , WL_c , 3) Q_c and WL_- , and 4) Q_c and WL_c with constant depth (2m) in the FB. (C) Sediment deposition in the 1m SS with TSS concentration 100 mg/l according the same four scenarios in B.

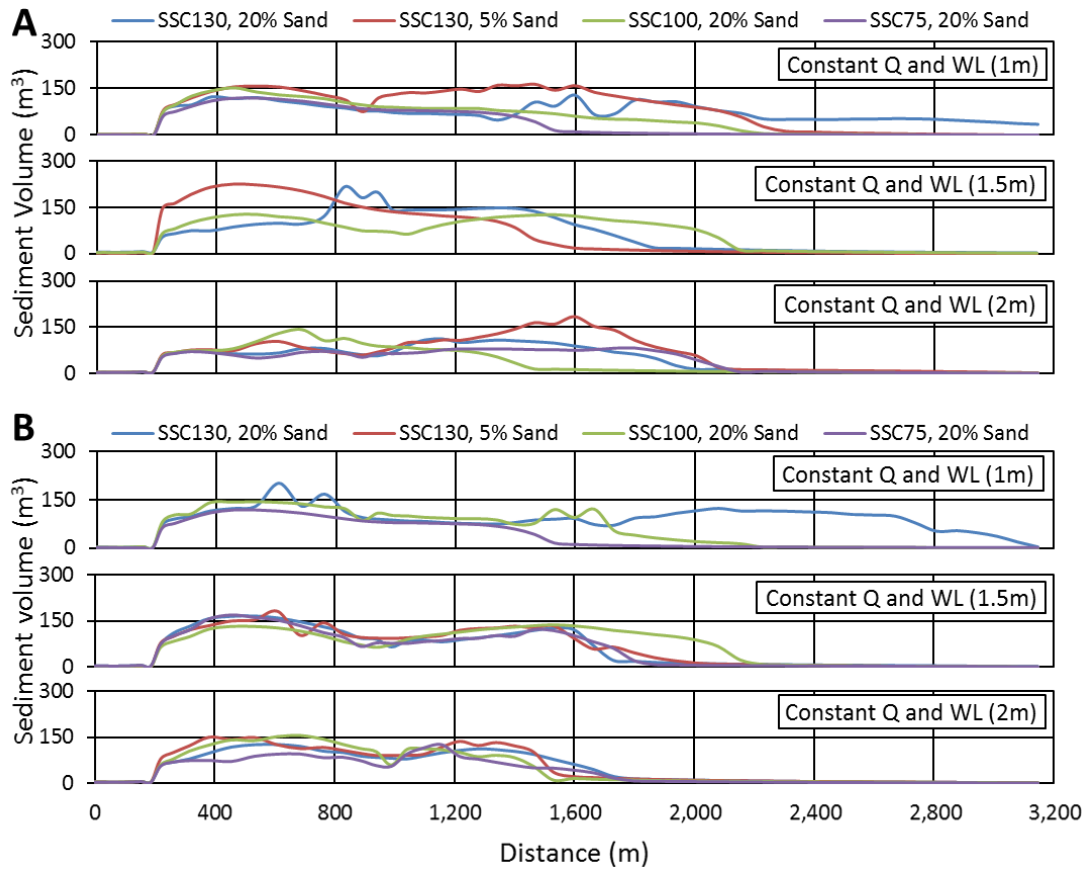


Figure 14: Relative sediment deposition volume including morph factor along the centerline of the basin per each sediment supply characteristic (SSC130, 20% sand [blue], SSC130, 5% sand [red], SSC100, 20% sand [green], SSC75, 20% sand [purple]). (A) Q_c and WL_c for each accommodation depth (1m, 1.5m, and 2m) in the FB. (B) Q_c and WL_c for each accommodation depth (1m, 1.5m, and 2m) in the HB.

Assessing the shape of the deposit over time, provides additional insight into factors that control the deposit volume and shape. Deposition in the undeveloped crevasse is proximal to the crevasse entrance during the first quarter of the simulation. By the second and third quarters, channelization has taken place that promotes deposition further basinward, away from the crevasse entrance. By the end of the simulation deposition has extended through the entire receiving basin and beyond the downstream boundary (Figure 15). The developed crevasse shows some deposition in the channel, likely due to channel initial size, but most of the deposition starts approximately 1,100m basinward of the crevasse entrance in the first and

second quarters of the simulation. By the third quarter the channel has almost reached the downstream boundary promoting deposition deep into the basin, and at the end of the simulation deposition has equally extended beyond the downstream boundary (Figure 15).

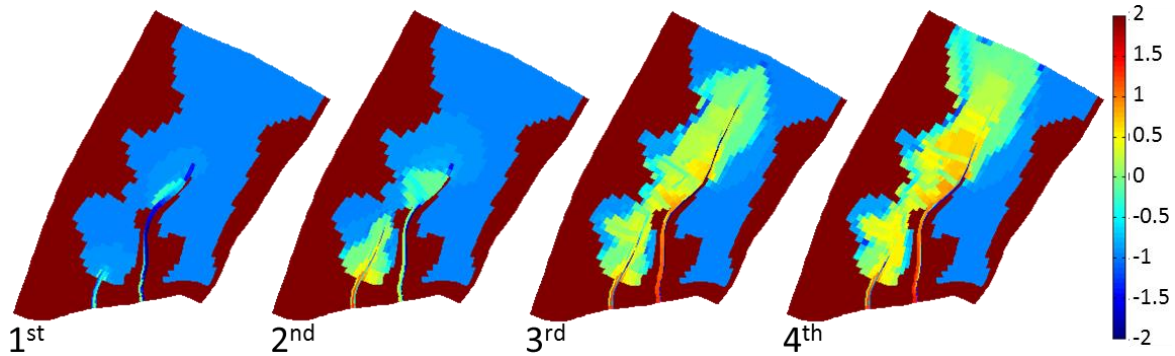


Figure 15: The evolution of ediment deposition in the 1m SS basin though out the simulation (1st, 2nd, 3rd and 4th quarters).

4.7 Sediment Retention

Model simulation results are used to infer sediment volume retention, where possible, based on differencing the cumulative sediment volume flux into the basin at the crevasse entrance, from the cumulative sediment volume flux exiting the basin (Figure 16). The type of sediment retained (sand, silt, or clay) are assessed based on sediment volumes retained in each fraction. The basin with an accommodation depth of 2m retained an average of 91% of the total sediment input, with similar retention percent in each class (100% of the sand, 95% of the silt and 85% of the clay). When evaluating Q and WL, an average of 94% of the sediment is retained in scenarios where WL remains constant and 92% in scenarios where Q remains constant. Sediment characteristics (SSC and sand fractions) did not have a big impact on sediment retention. The average retention was 93% when SSC was 130 and the sand fraction was 20% and 94% when SSC was 130 with 5% sand fraction. Average retention was 92% for both SSC 100 and SSC 75, both had 20% sand (Figure 16).

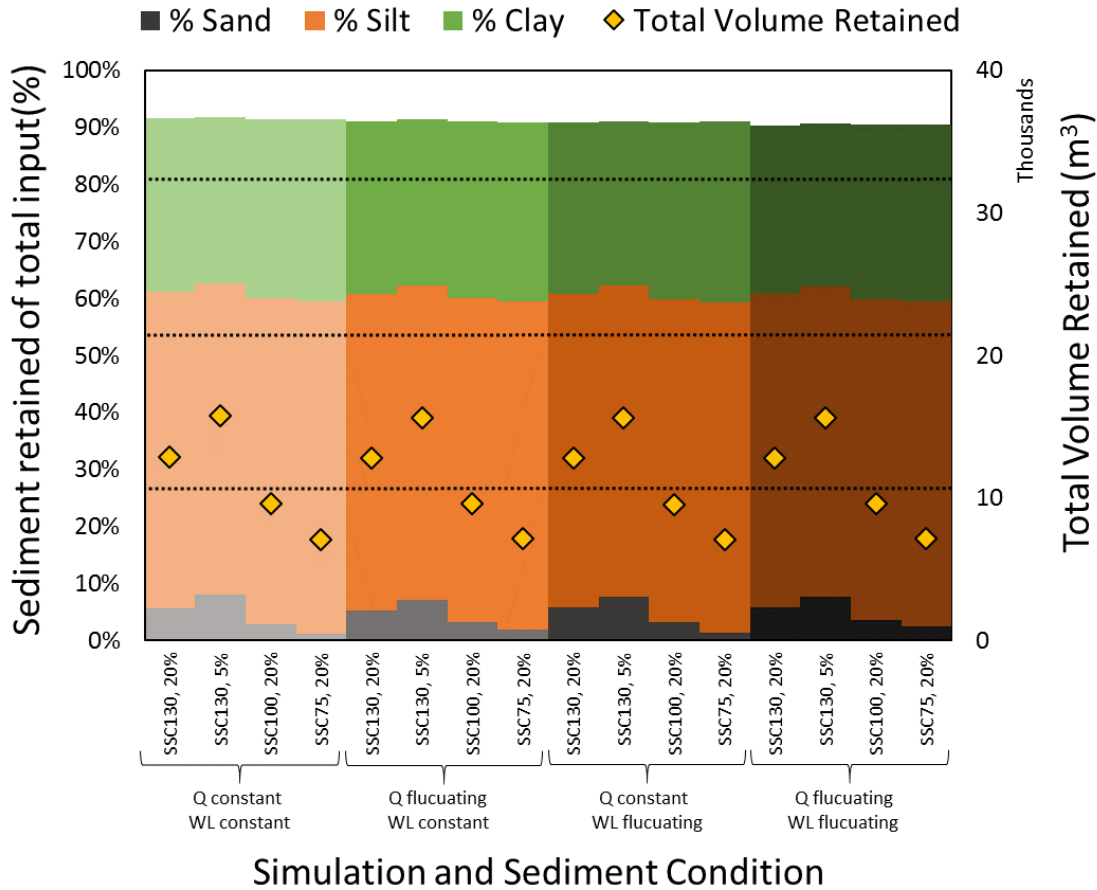


Figure 16: Sediment retained by percent (y-axis) and volume (secondary y-axis, yellow diamond) of total sediment input. Columns colors indicate what percent of the total percent sediment retained is sand (gray), silt (orange) or clay (green). Columns are further arranged by basin depth (1.5m and 2m), simulation type (Q_c, Q_f, WL_c, WL_f) and sediment condition at the input boundary (SSC, and % sand).

To assess sediment retention and channel competency as a function of the developing delta, as it becomes more established, we ran six, 15 day simulations for three delta morphologies, one with a developed delta (end point) and one that was partially developed (half way point). The simulations tested systems with existing planform geometry (SS, 1m depth), and two open basin accommodation depths (FB, 1m and 1.5m). The FB results exhibit a trend whereby sediment retention decreases as a function of delta development. Figure 17A,B shows that while sand retention is 100% throughout the experiment silt and clay retention changes from 96% to 84% (silt) and 88% to 65% (clay) from the half way point to the end of the experiment.

As accommodation depth increases (from 1 to 1.5m; Figure 17E,F) delta shape changes as does sediment retention. Sand retention remains at 100% throughout the experiment, while silt and clay retention remains unchanged (92% to 93% [silt] and 81% to 82% [clay] from the half way point to the end of the experiment); overall an increase in accommodation depth retains more silt and clay for the duration of this experiment. In a confined setting (SS) with a 1m accommodation depth sediment retention characteristics slightly increase although small, with silt and clay retention from 92% to 94% [silt] and 79% to 84% [clay] from the half way point to the end of the experiment (Figure 17C, D). Changes in planform geometry and accommodation depth produced similar response; each maintained overall higher retention rates for silt and clay for the duration of the experiment.

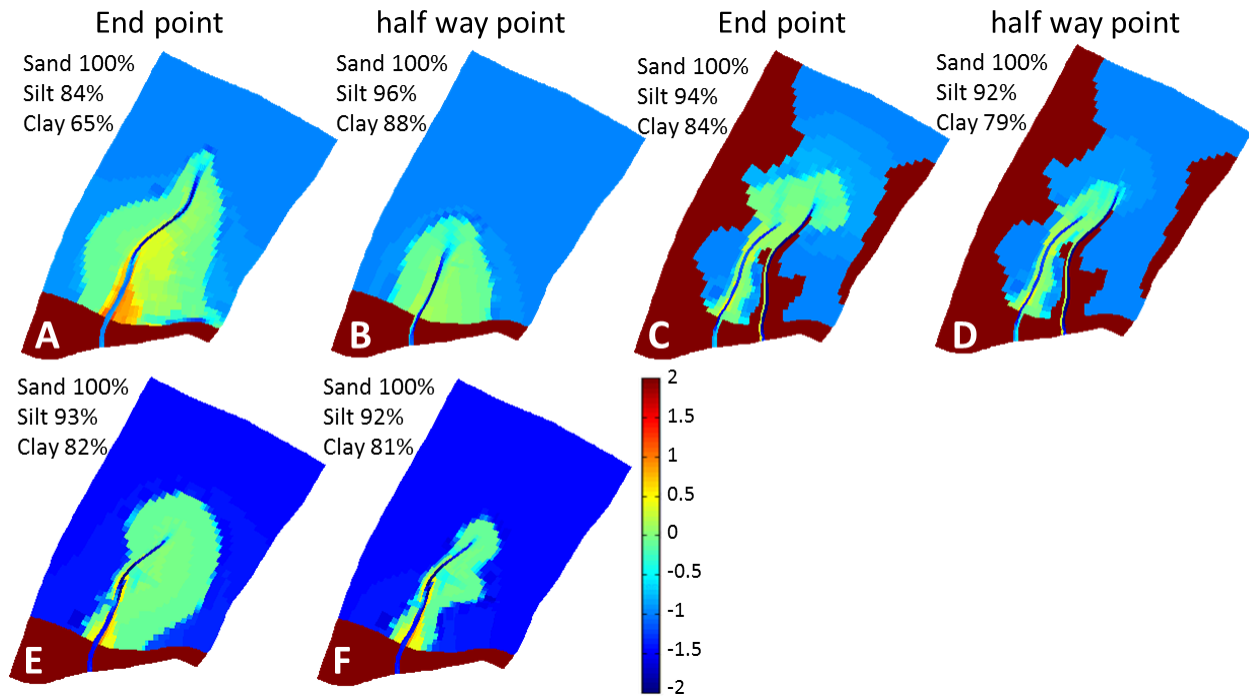


Figure 17: Fifteen-day simulation results using the end and half way points of the 1m SS, 1m and 1.5m FB simulations.

Discussion

First question: Do sub-delta crevasses follow delta growth laws?

Sub-delta crevasses in the MRD follow most of the delta growth laws with the exception of the non-dimensional distance to river mouth (Edmonds and Slingerland, 2007) and wetted allometry metrics (Wolinsky et al., 2010). The power law equation (Eq. 1) presented by Edmonds and Slingerland (2007) tends to predict a shorter non-dimensional distance to river mouth bar than what was measured in the SDC, TDB_13 (weakly cohesive), and the second order bifurcations of TDB_12 (strongly cohesive). The SDC typically have long channels relative to depth, with one to two bifurcations (Figure 18A-C; Figure 19A-E) a behavior that was also observed in the experimental deltas. The SDC and experimental deltas do demonstrate a systematic decrease of non-dimensional channel geometries (width, depth, and length) with increased bifurcation order, similar to large river dominated deltas (Figure 6; Mikhailov, 1970; Andren, 1994; Edmonds and Slingerland, 2007). This indicates that channels are adjusting to decreased flow (Edmonds and Slingerland, 2007), when bifurcations occur. However, the channel geometries decrease more rapidly per bifurcation order, most importantly the non-dimensional depth. This rapid decline in depth is also reflected in the width depth relationship (Figure 8) as a slight non-linearity.

It's important to recognize that a major difference between the SDC and Edmonds and Slingerland (2007) large deltas is sediment cohesion. A number of studies emphasize the importance of sediment cohesion on delta morphology (Hoyal and Sheets, 2009; Edmonds and

Slingerland, 2010; Caldwell and Edmonds, 2014; Straub et al., 2015). The greatest number of bifurcations form at an intermediate cohesion (Edmonds and Slingerland, 2010), with increasing sediment cohesion channel banks strengthen, channel mobility reduces, and channels deepen (Straub et al., 2015). High mud content and vegetation has been recognized as a stabilizing mechanism of levees (Edmonds and Slingerland, 2010; Canestrelli et al., 2014) and could indirectly promote the formation of a levee dominated river mouth since the bed would likely be smoother, leading to a reduction of friction and jet spreading (Canestrelli et al., 2014). This is seen in TDB_12 (strongly cohesive) delta, where there are fewer but deeper channels (Straub et al., 2015). The SDC have long channels but they are relatively shallow. This suggests that the SDC are intermediate to strongly cohesive, where bifurcations are limited, channel lengths are long and depths are shallow (Figure 18) or that cohesion is not the only factor controlling the excess lengths of the channels (i.e. receiving basin characteristics, discussed later).

Cohesive deltas are also characterized by low-wetted area (Hoyal and Sheets, 2009). This explains why the SDC exhibit similar delta land allometry scaling (Figure 7A and B), but not all of the crevasses displayed fractal growth of the wetted allometry (Figure 7C). Less channel splitting (i.e. bifurcations) in some crevasses causes channel extension to create wetted perimeter faster than or at the same rate as wetted area. Both of the experimental deltas had high land allometry scaling (Figure 7D and E). This is likely due to the fact that the digitized data began with an already established delta, therefore the delta area stays relatively constant though out time, oscillating as the delta naturally reorganizes. The experimental deltas also did not follow the wetted allometry scaling (Figure 7F). This could be an artifact of where the water level was interpreted to be during the image analysis.

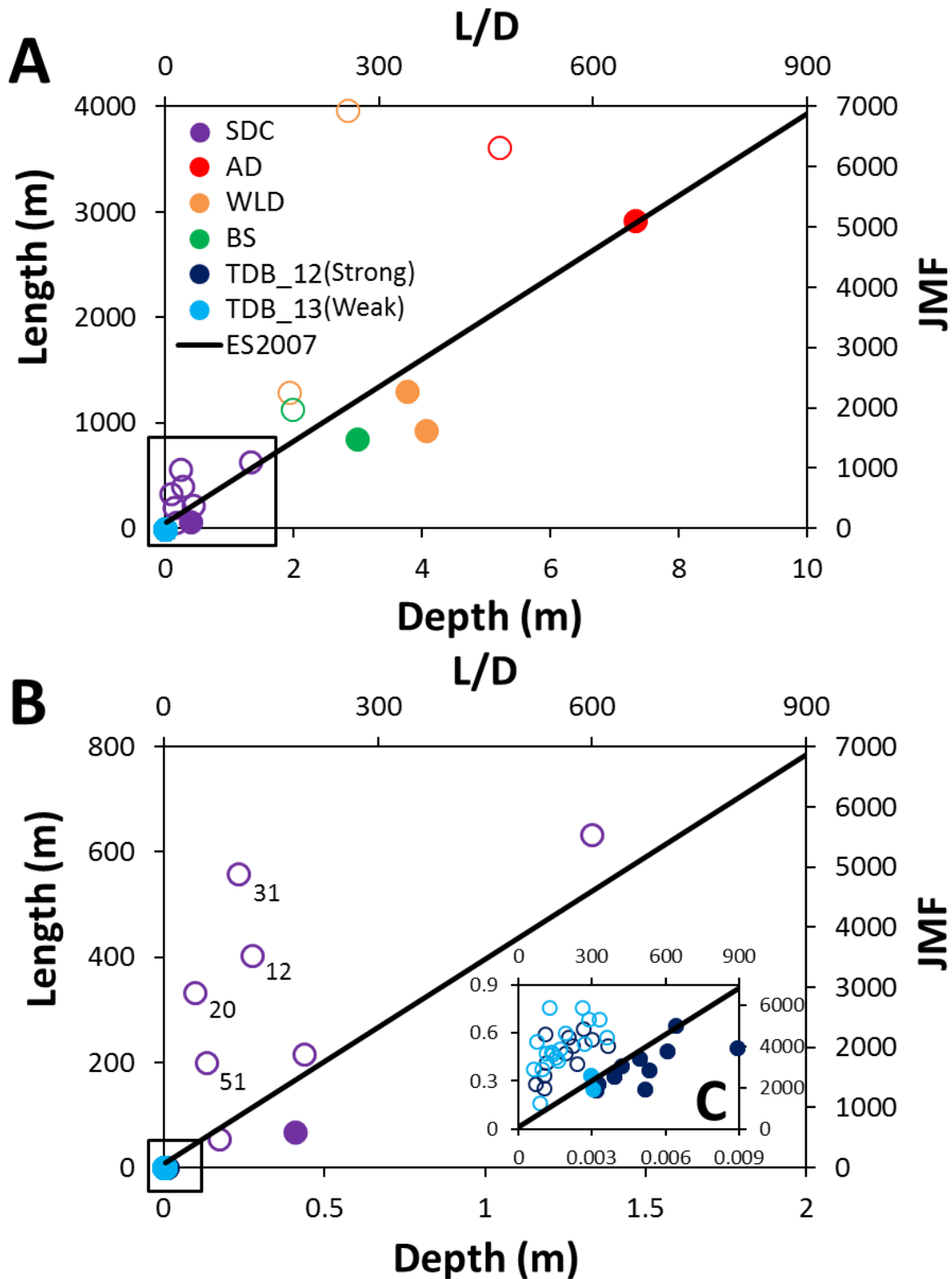


Figure 18: Length to depth relationship for AD (red), WLD (orange), Brant's Splay (BS; green), SDC (purple), TDB_12 (dark blue), and TDB_13 (light blue). Open circles indicate when the predicted length (L_{RMB}/D) was shorter than the measured (L/D). The solid circles indicate when the predicted was longer than measured. The black line on the secondary x and y-axis is the Edmonds and Slingerland (2007) trend.

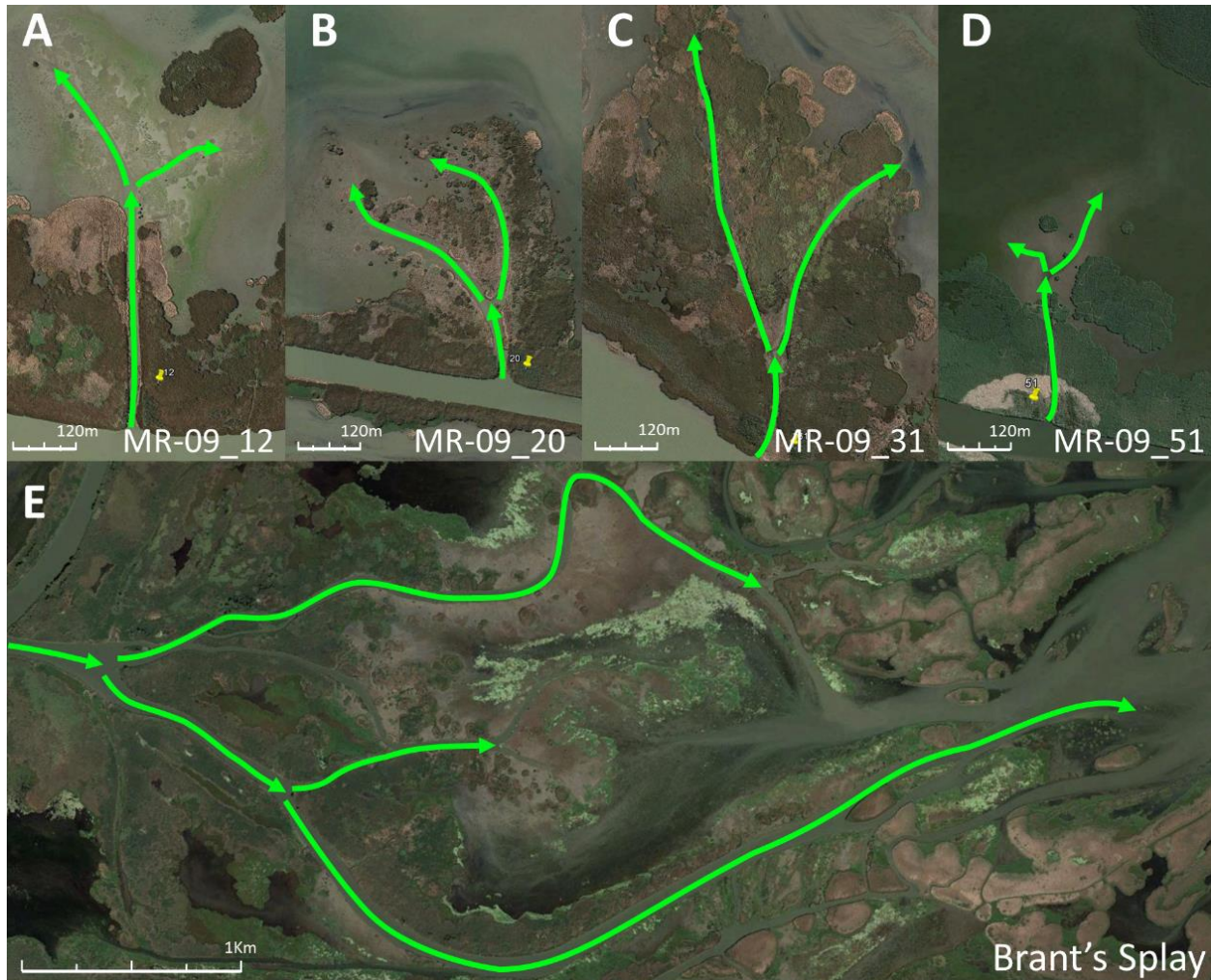


Figure 19: The SDC (12, 20, 31 and 51; A-D) and Brant's Splay (E), showcasing the low number of bifurcations and channel lengths.

Second question: Is the competency of the channel network to carry sediments is governed by the channel network and basin geometry?

Model results suggest that SDC do exhibit basinward migration as a function of SDC development (Figure 15). In strongly cohesive deltas the highly concentrated jet created by erosion resistant levees and narrow channel recycles the mouth bar basinward causing channel progradation into the basin (Parker, 1978; Edmonds and Slingerland, 2010). Model results also suggest that SDC do exhibit asymmetric channel network growth when subjected to a change in

receiving basin characteristics. We found that slightly more bifurcations occurred in the 1m basins compared to basins with 1.5 and 2m. This is likely a simulation time issue, where deeper basins need longer run time to build a comparable delta to the 1m basin because of the increased accommodation depth. It's possible that they would have had the same result given more time. Although accommodation depth seemingly did not have a large effect on asymmetric channel growth, planform geometry did. The open basins (FB and HB) usually experienced bifurcations, while the SS rarely bifurcated. This suggests that limited lateral accommodation in the sub-delta crevasses due to the receiving basin geometry is a contributing, if not the dominant factor in the asymmetric growth of SDC.

In the shallow open basin, mud retention decreased as a function of delta development (Figure 17A-B), but remained the same as delta developed in the deeper open basin (Figure 17E-F). It is likely that if the deeper open basin had continued to develop, mud retention would have decreased. Enhanced channelization resulting from sediment cohesion also increases the pumping of fine-grained sediment basinward, where it can bypass the delta foreset, decreasing total delta sediment retention rate (Straub et al., 2015). In a confined basin, however mud retention slightly increased as a function of delta development (Figure 17C-D), suggesting that receiving basin geometry also a dominant factor in sediment retention, which further contributes to asymmetric growth.

Conclusions

The growth of sub-delta crevasses within the Mississippi River Delta is similar to large river dominated deltas. They exhibit a systematic decrease of non-dimensional channel geometries with increased bifurcation order. They have almost linear evolution of land allometry and they have a linear relationship between width and depth. However, long channel lengths and limited bifurcations, cause the non-dimensional distance to river mouth bar to be larger with a lower jet momentum flux and contribute to low wetted allometry growth in some crevasses. These long lengths and limited bifurcations (i.e. asymmetric growth) are the result of sediment cohesion due to mud content and limited lateral accommodation of receiving basin geometry. Sub-delta crevasses exhibit basinward migration as a function of delta development which is also a result of sediment cohesion and receiving basin geometry. Receiving basin geometry in turn increases retention of mud with delta development further contributing to asymmetric growth. These results provide insight into how crevasses transport, deposit, and retain sediment. Future research should focus on how different receiving basin geometries influence crevasse growth and further investigate upstream or downstream controls.

References

- Andrén, H. (1994). Development of the Laitaure delta. *Swedish lappland: A study of growth, distributary forms, and processes.*
- Allison, M. A., & Meselhe, E. A. (2010). The use of large water and sediment diversions in the lower Mississippi River (Louisiana) for coastal restoration. *Journal of Hydrology*, 387(3), 346-360.
- ASTM. 1997. Standard test methods for determining sediment concentration in water samples. ASTM D 3977-97.
- Bagnold, R. A. (1966). An approach to the sediment transport problem. *General Physics Geological Survey, Prof. paper.*
- Bates, C. C. (1953). Rational theory of delta formation. *AAPG Bulletin*, 37(9), 2119-2162.
- Blum, M. D., & Roberts, H. H. (2012). The Mississippi delta region: past, present, and future. *Annual Review of Earth and Planetary Sciences*, 40, 655-683.
- Blum, M. D., & Roberts, H. H. (2009). Drowning of the Mississippi Delta due to insufficient sediment supply and global sea-level rise. *Nature Geoscience*, 2(7), 488-491.
- Boyer, M. E., & Harris, J. O. R. Eugene Turner, 1997. Constructed Crevasses and Land Gain in the Mississippi River Delta. *Restoration Ecology*, 5, 85-92.
- Caldwell, R. L., & Edmonds, D. A. (2014). The effects of sediment properties on deltaic processes and morphologies: A numerical modeling study. *Journal of Geophysical Research: Earth Surface*, 119(5), 961-982.

- Canestrelli, A., Nardin, W., Edmonds, D., Fagherazzi, S., & Slingerland, R. (2014). Importance of frictional effects and jet instability on the morphodynamics of river mouth bars and levees. *Journal of Geophysical Research: Oceans*, 119(1), 509-522.
- Carter, M. R. (Ed.). (1993). *Soil sampling and methods of analysis*. CRC Press.
- Chow, V. T. "Open-Channel Hydraulics McGraw-Hill Kagakusha Ltd." International Student Edition (1956).
- Church, J. A., & White, N. J. (2006). A 20th century acceleration in global sea-level rise. *Geophysical research letters*, 33(1).
- Clark, R.B., Georgiou, I.Y., FitzGerald, D.M., (2013). An Evolutionary Model of a Retrograding Subdeltaic Distributary of a River-Dominated System, Abstracts with Programs, Presentation at the Association for the Sciences of Limnology and Oceanography - ASLO, February 17 – 22, New Orleans, LA.
- Couvillion, B. R., Barras, J. A., Steyer, G. D., Sleavin, W., Fischer, M., Beck, H., & Heckman, D. (2011). *Land area change in coastal Louisiana (1932 to 2010)* (pp. 1-12). US Department of the Interior, US Geological Survey.
- Day, J. W., Boesch, D. F., Clairain, E. J., Kemp, G. P., Laska, S. B., Mitsch, W. J., ... & Simenstad, C. A. (2007). Restoration of the Mississippi Delta: lessons from hurricanes Katrina and Rita. *science*, 315(5819), 1679-1684.
- Deltares (2015) Delft3D; Simulation of Multi-Dimensional Hydrodynamic Flows and Transport Phenomena, Including Sediments, Hydro-Morphodynamics; Deltares: Delft, The Netherlands.
- Dokka, R. K. (2006). Modern-day tectonic subsidence in coastal Louisiana. *Geology*, 34(4), 281-284.

- Donnelly, J. P., Cleary, P., Newby, P., & Ettinger, R. (2004). Coupling instrumental and geological records of sea-level change: evidence from southern New England of an increase in the rate of sea-level rise in the late 19th century. *Geophysical Research Letters*, 31(5).
- Edmonds, D. A., & Slingerland, R. L. (2007). Mechanics of river mouth bar formation: Implications for the morphodynamics of delta distributary networks. *Journal of Geophysical Research: Earth Surface*, 112(F2).
- Edmonds, D. A. (2012). Restoration sedimentology. *Nature Geoscience*, 5(11), 758-759.
- Edmonds, D. A., Paola, C., Hoyal, D. C., & Sheets, B. A. (2011). Quantitative metrics that describe river deltas and their channel networks. *Journal of Geophysical Research: Earth Surface*, 116(F4).
- Esposito, C. R., Georgiou, I. Y., & Kolker, A. S. (2013). Hydrodynamic and geomorphic controls on mouth bar evolution. *Geophysical Research Letters*, 40(8), 1540-1545.
- Fagherazzi, S., Bortoluzzi, A., Dietrich, W. E., Adami, A., Lanzoni, S., Marani, M., & Rinaldo, A. (1999). Tidal networks: 1. Automatic network extraction and preliminary scaling features from digital terrain maps. *Water Resources Research*, 35(12), 3891-3904.
- Gagliano, S. M., van Beek, J., 1975. An approach to multi-use management in the Mississippi Delta System. In: Broussard, M.L. (Ed.), *Deltas: Models for Exploration*, Houston, pp. 223-238.
- Geleynse, N., Storms, J. E., Walstra, D. J. R., Jagers, H. A., Wang, Z. B., & Stive, M. J. (2011). Controls on river delta formation; insights from numerical modelling. *Earth and Planetary Science Letters*, 302(1), 217-226.

- Giosan, L., Syvitski, J., Constantinescu, S., & Day, J. (2014). Climate change: protect the world's deltas. *Nature*, 516(7529), 31-33.
- Hack, J. T. (1957). *Studies of longitudinal stream profiles in Virginia and Maryland* (Vol. 294). US Government Printing Office.
- Hanegan, K. C. (2011). *Modeling the Evolution of the Wax Lake Delta in Atchafalaya Bay, Louisiana* (Doctoral dissertation, TU Delft, Delft University of Technology).
- Hansson, S. V., Kaste, J. M., Chen, K., & Bindler, R. (2014). Beryllium-7 as a natural tracer for short-term downwash in peat. *Biogeochemistry*, 119(1-3), 329-339.
- Howes, N. C., Georgiou, I. Y., Hughes, Z. J., & Wolinsky, M. A. (2012, December). A Conceptual Framework and Classification for the Fluvial-Backwater-Marine Transition in Coastal Rivers Globally. In *AGU Fall Meeting Abstracts* (Vol. 1, p. 01).
- Hoyal, D. C. J. D., & Sheets, B. A. (2009). Morphodynamic evolution of experimental cohesive deltas. *Journal of Geophysical Research: Earth Surface*, 114(F2).
- Ikeda, S. (1982). Incipient motion of sand particles on side slopes. *Journal of the Hydraulics Division*, 108(1), 95-114.
- Kim, W., Mohrig, D., Twilley, R., Paola, C., & Parker, G. (2009). Is it feasible to build new land in the Mississippi River Delta. *Eos*, 90(42), 373-374.
- Lesser, M. P., Weis, V. M., Patterson, M. R., & Jokiel, P. L. (1994). Effects of morphology and water motion on carbon delivery and productivity in the reef coral, *Pocillopora damicornis* (Linnaeus): diffusion barriers, inorganic carbon limitation, and biochemical plasticity. *Journal of Experimental Marine Biology and Ecology*, 178(2), 153-179.
- Li, Q., Lu, L., & Straub, K. M. (2016). Storage thresholds for relative sea-level signals in the stratigraphic record. *Geology*, G37484-1.

- Liang, M., Van Dyk, C., & Passalacqua, P. (2016). Quantifying the patterns and dynamics of river deltas under conditions of steady forcing and relative sea level rise. *Journal of Geophysical Research: Earth Surface*.
- Liang, M., Voller, V. R., & Paola, C. (2015). A reduced-complexity model for river delta formation—Part 1: Modeling deltas with channel dynamics. *Earth Surface Dynamics*, 3(1), 67-86.
- Meselhe, E. A., Georgiou, I., Allison, M. A., & McCorquodale, J. A. (2012). Numerical modeling of hydrodynamics and sediment transport in lower Mississippi at a proposed delta building diversion. *Journal of Hydrology*, 472, 340-354.
- Mikhailov, V. N. (1970). Hydrologic-morphometric characteristics of delta branches. *Stud. Rep. Hydrol*, 9, 146-158.
- Paola, C., Straub, K., Mohrig, D., & Reinhardt, L. (2009). The “unreasonable effectiveness” of stratigraphic and geomorphic experiments. *Earth-Science Reviews*, 97(1), 1-43.
- Paola, C., Twilley, R. R., Edmonds, D. A., Kim, W., Mohrig, D., Parker, G., ... & Voller, V. R. (2011). Natural processes in delta restoration: Application to the Mississippi Delta. *Annual Review of Marine Science*, 3, 67-91.
- Parker, G., Toro-Escobar, C. M., Ramey, M., & Beck, S. (2003). Effect of floodwater extraction on mountain stream morphology. *Journal of Hydraulic Engineering*, 129(11), 885-895.
- Partheniades, E. (1965). Erosion and deposition of cohesive soils. *Journal of the Hydraulics Division*, 91(1), 105-139.
- Rinaldo, A., Fagherazzi, S., Lanzoni, S., Marani, M., & Dietrich, W. E. (1999). Tidal networks 2. Watershed delineation and comparative network morphology. *Water Resources Research*, 35(12), 3905-3917.

- Snedden, G. A., Cable, J. E., Swarzenski, C., & Swenson, E. (2007). Sediment discharge into a subsiding Louisiana deltaic estuary through a Mississippi River diversion. *Estuarine, Coastal and Shelf Science*, 71(1), 181-193.
- Shaw, J. B., Mohrig, D., & Whitman, S. K. (2013). The morphology and evolution of channels on the Wax Lake Delta, Louisiana, USA. *Journal of Geophysical Research: Earth Surface*, 118(3), 1562-1584.
- Straub, K. M., & Esposito, C. R. (2013). Influence of water and sediment supply on the stratigraphic record of alluvial fans and deltas: Process controls on stratigraphic completeness. *Journal of Geophysical Research: Earth Surface*, 118(2), 625-637.
- Straub, K. M., Jerolmack, D. J., Mohrig, D., & Rothman, D. H. (2007). Channel network scaling laws in submarine basins. *Geophysical Research Letters*, 34(12).
- Straub, K. M., Li, Q., & Benson, W. M. (2015). Influence of sediment cohesion on deltaic shoreline dynamics and bulk sediment retention: A laboratory study. *Geophysical Research Letters*, 42(22), 9808-9815.
- Stokes, George Gabriel. *On the effect of the internal friction of fluids on the motion of pendulums*. Vol. 9. Pitt Press, 1851.
- Syvitski, J. P., & Saito, Y. (2007). Morphodynamics of deltas under the influence of humans. *Global and Planetary Change*, 57(3), 261-282.
- Törnqvist, T. E., Wallace, D. J., Storms, J. E., Wallinga, J., Van Dam, R. L., Blaauw, M., ... & Snijders, E. M. (2008). Mississippi Delta subsidence primarily caused by compaction of Holocene strata. *Nature Geoscience*, 1(3), 173-176.
- Turner, R. E., & Boyer, M. E. (1997). Mississippi River diversions, coastal wetland restoration/creation and an economy of scale. *Ecological Engineering*, 8(2), 117-128.

- Van Rijn, L. C. (1993). *Principles of sediment transport in rivers, estuaries and coastal seas* (Vol. 1006). Amsterdam: Aqua publications.
- Welder, F. A. (1959). *Processes of deltaic sedimentation in the lower Mississippi River* (No. TR12C59 7). COAST PRO-SEAL AND MFG CO LOS ANGELES CA.
- Wolinsky, M. A., Edmonds, D. A., Martin, J., & Paola, C. (2010). Delta allometry: Growth laws for river deltas. *Geophysical Research Letters*, 37(21).
- Wright, L. D., & Coleman, J. M. (1974). Mississippi River mouth processes: effluent dynamics and morphologic development. *The Journal of Geology*, 751-778.
- Wright, L. D. (1977). Sediment transport and deposition at river mouths: a synthesis. *Geological Society of America Bulletin*, 88(6), 857-868.
- Yocum, T., & Georgiou, I. Y. (2014). Do Constructed Crevasses Obey Delta Laws? Implications for the Restoration of the Mississippi River Delta. *Ecology*, 5(1), 85-92.

Appendix A

Case names: Case, and Simulation name	Depth (m)	DS/RB WL	UDC Q (m³/s)	DC Q (m³/s)	Downstream Boundary	Morph Factor	Sand (%)	Silt (%)	Clay (%)	TSS (mg/l)
Case B1 noOP	1	0	21	46	Full	10	20%	50%	30%	130
Case B1 5% sand	1	0	21	46	Full	10	5%	60%	35%	130
Case B1 TSS100	1	0	21	46	Full	10	20%	50%	30%	100
Case B1 TSS75	1	0	21	46	Full	10	20%	50%	30%	75
Case B2	1	0	~	~	Full	10	20%	50%	30%	130
Case B2 5% sand	1	0	~	~	Full	10	5%	60%	35%	130
Case B2 TSS100	1	0	~	~	Full	10	20%	50%	30%	100
Case B2 TSS75	1	0	~	~	Full	10	20%	50%	30%	75
Case B3	1	~	21	46	Full	10	20%	50%	30%	130
Case B3 5% sand	1	~	21	46	Full	10	5%	60%	35%	130
Case B3 TSS100	1	~	21	46	Full	10	20%	50%	30%	100
Case B3 TSS75	1	~	21	46	Full	10	20%	50%	30%	75
Case B1	1.5	0	21	46	Full	10	20%	50%	30%	130
Case B1 5% sand	1.5	0	21	46	Full	10	5%	60%	35%	130
Case B1 TSS100	1.5	0	21	46	Full	10	20%	50%	30%	100
Case B1 TSS75	1.5	0	21	46	Full	10	20%	50%	30%	75
Case B2	1.5	0	~	~	Full	10	20%	50%	30%	130
Case B2 5% sand	1.5	0	~	~	Full	10	5%	60%	35%	130
Case B2 TSS100	1.5	0	~	~	Full	10	20%	50%	30%	100
Case B2 TSS75	1.5	0	~	~	Full	10	20%	50%	30%	75
Case B3	1.5	~	21	46	Full	10	20%	50%	30%	130
Case B3 5% sand	1.5	~	21	46	Full	10	5%	60%	35%	130
Case B3 TSS100	1.5	~	21	46	Full	10	20%	50%	30%	100
Case B3 TSS75	1.5	~	21	46	Full	10	20%	50%	30%	75
Case B1 noOP	2	0	21	46	Full	10	20%	50%	30%	130
Case B1 5% sand	2	0	21	46	Full	10	5%	60%	35%	130
Case B1 TSS100	2	0	21	46	Full	10	20%	50%	30%	100
Case B1 TSS75	2	0	21	46	Full	10	20%	50%	30%	75
Case B2	2	0	~	~	Full	10	20%	50%	30%	130
Case B2 5% sand	2	0	~	~	Full	10	5%	60%	35%	130
Case B2 TSS100	2	0	~	~	Full	10	20%	50%	30%	100
Case B2 TSS75	2	0	~	~	Full	10	20%	50%	30%	75

Case B3	2	~	21	46	Full	10	20%	50%	30%	130
Case B3 5% sand	2	~	21	46	Full	10	5%	60%	35%	130
Case B3 TSS100	2	~	21	46	Full	10	20%	50%	30%	100
Case B3 TSS75	2	~	21	46	Full	10	20%	50%	30%	75
Case C1	1	0	21	N/A	Full	25	20%	50%	30%	130
Case C1	1	0	67	N/A	Full	10	20%	50%	30%	130
Case C1 5% sand	1	0	67	N/A	Full	10	5%	60%	35%	130
Case C1 TSS100	1	0	67	N/A	Full	10	20%	50%	30%	100
Case C1 TSS75	1	0	67	N/A	Full	10	20%	50%	30%	75
Case C2	1	0	~	N/A	Full	10	20%	50%	30%	130
Case C2 5% sand	1	0	~	N/A	Full	10	5%	60%	35%	130
Case C2 TSS100	1	0	~	N/A	Full	10	20%	50%	30%	100
Case C2 TSS75	1	0	~	N/A	Full	10	20%	50%	30%	75
Case C3	1	~	67	N/A	Full	10	20%	50%	30%	130
Case C3 TSS75	1	~	67	N/A	Full	1	20%	50%	30%	75
Case C3 5% sand	1	~	67	N/A	Full	10	5%	60%	35%	130
Case C3 TSS100	1	~	67	N/A	Full	10	20%	50%	30%	100
Case C3 TSS75 m10	1	~	67	N/A	Full	10	20%	50%	30%	75
Case C4	1	~	~	N/A	Full	10	20%	50%	30%	130
Case C4 5% sand	1	~	~	N/A	Full	10	5%	60%	35%	130
Case C4 TSS100	1	~	~	N/A	Full	10	20%	50%	30%	100
Case C4 TSS75	1	~	~	N/A	Full	10	20%	50%	30%	75
Case C1	1.5	0	67	N/A	Full	10	20%	50%	30%	130
Case C1 5% sand	1.5	0	67	N/A	Full	10	5%	60%	35%	130
Case C1 TSS100	1.5	0	67	N/A	Full	10	20%	50%	30%	100
Case C1 TSS75	1.5	0	67	N/A	Full	10	20%	50%	30%	75
Case C2	1.5	0	~	N/A	Full	10	20%	50%	30%	130
Case C2 5% sand	1.5	0	~	N/A	Full	10	5%	60%	35%	130
Case C2 TSS100	1.5	0	~	N/A	Full	10	20%	50%	30%	100
Case C2 TSS75	1.5	0	~	N/A	Full	10	20%	50%	30%	75
Case C3	1.5	~	67	N/A	Full	10	20%	50%	30%	130
Case C3 5% sand	1.5	~	67	N/A	Full	10	5%	60%	35%	130
Case C3 TSS100	1.5	~	67	N/A	Full	10	20%	50%	30%	100
Case C3 TSS75	1.5	~	67	N/A	Full	10	20%	50%	30%	75
Case C4	1.5	~	~	N/A	Full	10	20%	50%	30%	130
Case C4 5% sand	1.5	~	~	N/A	Full	10	5%	60%	35%	130
Case C4 TSS100	1.5	~	~	N/A	Full	10	20%	50%	30%	100

Case C4 TSS75	1.5	~	~	N/A	Full	10	20%	50%	30%	75
Case C1 noOP	2	0	21	N/A	Full	25	20%	50%	30%	130
Case C1	2	0	67	N/A	Full	10	20%	50%	30%	130
Case C1 5%sand	2	0	67	N/A	Full	10	5%	60%	35%	130
Case C1 TSS100	2	0	67	N/A	Full	10	20%	50%	30%	100
Case C1 TSS75	2	0	67	N/A	Full	10	20%	50%	30%	75
Case C2	2	0	~	N/A	Full	10	20%	50%	30%	130
Case C2 5%sand	2	0	~	N/A	Full	10	5%	60%	35%	130
Case C2 TSS100	2	0	~	N/A	Full	10	20%	50%	30%	100
Case C2 TSS75	2	0	~	N/A	Full	10	20%	50%	30%	75
Case C3	2	~	67	N/A	Full	10	20%	50%	30%	130
Case C3 TSS75	2	~	67	N/A	Full	1	20%	50%	30%	75
Case C3 5%sand	2	~	67	N/A	Full	10	5%	60%	35%	130
Case C3 TSS100	2	~	67	N/A	Full	10	20%	50%	30%	100
Case C3 TSS75 m10	2	~	67	N/A	Full	10	20%	50%	30%	75
Case C4	2	~	~	N/A	Full	10	20%	50%	30%	130
Case C4 5%sand	2	~	~	N/A	Full	10	5%	60%	35%	130
Case C4 TSS100	2	~	~	N/A	Full	10	20%	50%	30%	100
Case C4 TSS75	2	~	~	N/A	Full	10	20%	50%	30%	75
Case D1 noOP	1	0	21	N/A	Half	25	20%	50%	30%	130
Case D1	1	0	67	N/A	Half	10	20%	50%	30%	130
Case D1 5%sand	1	0	67	N/A	Half	10	5%	60%	35%	130
Case D1 TSS100	1	0	67	N/A	Half	10	20%	50%	30%	100
Case D1 TSS75	1	0	67	N/A	Half	10	20%	50%	30%	75
Case D2	1	0	~	N/A	Half	10	20%	50%	30%	130
Case D2 5%sand	1	0	~	N/A	Half	10	5%	60%	35%	130
Case D2 TSS100	1	0	~	N/A	Half	10	20%	50%	30%	100
Case D2 TSS75	1	0	~	N/A	Half	10	20%	50%	30%	75
Case D3	1	~	67	N/A	Half	10	20%	50%	30%	130
Case D3 TSS75	1	~	67	N/A	Half	1	20%	50%	30%	75
Case D3 5%sand	1	~	67	N/A	Half	10	5%	60%	35%	130
Case D3 TSS100	1	~	67	N/A	Half	10	20%	50%	30%	100
Case D3 TSS75m10	1	~	67	N/A	Half	10	20%	50%	30%	75
Case D4	1	~	~	N/A	Half	10	20%	50%	30%	130
Case D4 5%sand	1	~	~	N/A	Half	10	5%	60%	35%	130
Case D4 TSS100	1	~	~	N/A	Half	10	20%	50%	30%	100

Case D4 TSS75	1	~	~	N/A	Half	10	20%	50%	30%	75
Case D1	1.5	0	67	N/A	Half	10	20%	50%	30%	130
Case D1 5% sand	1.5	0	67	N/A	Half	10	5%	60%	35%	130
Case D1 TSS100	1.5	0	67	N/A	Half	10	20%	50%	30%	100
Case D1 TSS75	1.5	0	67	N/A	Half	10	20%	50%	30%	75
Case D2	1.5	0	~	N/A	Full	10	20%	50%	30%	130
Case D2 5% sand	1.5	0	~	N/A	Full	10	5%	60%	35%	130
Case D2 TSS100	1.5	0	~	N/A	Full	10	20%	50%	30%	100
Case D2 TSS75	1.5	0	~	N/A	Full	10	20%	50%	30%	75
Case D3	1.5	~	67	N/A	Full	10	20%	50%	30%	130
Case D3 5% sand	1.5	~	67	N/A	Full	10	5%	60%	35%	130
Case D3 TSS100	1.5	~	67	N/A	Full	10	20%	50%	30%	100
Case D3 TSS75	1.5	~	67	N/A	Full	10	20%	50%	30%	75
Case D4	1.5	~	~	N/A	Full	10	20%	50%	30%	130
Case D4 5% sand	1.5	~	~	N/A	Full	10	5%	60%	35%	130
Case D4 TSS100	1.5	~	~	N/A	Full	10	20%	50%	30%	100
Case D4 TSS75	1.5	~	~	N/A	Full	10	20%	50%	30%	75
Case D1 noOP	2	0	21	N/A	Half	25	20%	50%	30%	130
Case D1	2	0	67	N/A	Half	10	20%	50%	30%	130
Case D1 5% sand	2	0	67	N/A	Half	10	5%	60%	35%	130
Case D1 TSS100	2	0	67	N/A	Half	10	20%	50%	30%	100
Case D1 TSS75	2	0	67	N/A	Half	10	20%	50%	30%	75
Case D2	2	0	~	N/A	Full	10	20%	50%	30%	130
Case D2 5% sand	2	0	~	N/A	Full	10	5%	60%	35%	130
Case D2 TSS100	2	0	~	N/A	Full	10	20%	50%	30%	100
Case D2 TSS75	2	0	~	N/A	Full	10	20%	50%	30%	75
Case D3	2	~	67	N/A	Full	10	20%	50%	30%	130
Case D3 TSS75	2	~	67	N/A	Full	1	20%	50%	30%	75
Case D3 5% sand	2	~	67	N/A	Full	10	5%	60%	35%	130
Case D3 TSS100	2	~	67	N/A	Full	10	20%	50%	30%	100
Case D3 TSS75	2	~	67	N/A	Full	10	20%	50%	30%	75
Case D4	2	~	~	N/A	Full	10	20%	50%	30%	130
Case D4 5% sand	2	~	~	N/A	Full	10	5%	60%	35%	130
Case D4 TSS100	2	~	~	N/A	Full	10	20%	50%	30%	100
Case D4 TSS75	2	~	~	N/A	Full	10	20%	50%	30%	75

Vita

Tara A. Yocum earned her Bachelor's Degree in 2014, majoring in Earth and Environmental Sciences at the University of New Orleans (UNO). As an undergraduate in early 2013, she began volunteering in the Hydrodynamics and Sediment transport laboratory under the advisement of Dr. Ioannis Georgiou. The following year she was given the opportunity to become an undergraduate student worker with Dr. Ioannis Georgiou and the Pontchartrain Institute for Environmental Sciences. In the spring of 2015 she joined the UNO Earth and Environmental Science Masters' program as a Graduate Research Assistant.